





## Quantum coherent control in pulsed waveguide optomechanics

Junyin Zhang <sup>1,2</sup> Changlong Zhu <sup>1,3</sup> Christian Wolff <sup>4</sup> and Birgit Stiller <sup>1,3,\*</sup>

<sup>1</sup>Max Planck Institute for the Science of Light, Staudtstr. 2, 91058 Erlangen, Germany

<sup>2</sup>Department of Physics, University of Science and Technology of China, 230026 Hefei, China

<sup>3</sup>Department of Physics, University of Erlangen-Nuremberg, Staudtstr. 7, 91058 Erlangen, Germany

<sup>4</sup>Centre for Nano Optics, University of Southern Denmark, Campusvej 55, DK-5230 Odense M, Denmark



(Received 31 March 2022; accepted 16 November 2022; published 11 January 2023)

Coherent control of traveling acoustic excitations in a waveguide system is an interesting way to manipulate and transduce classical and quantum information. So far, these interactions, often based on optomechanical resonators or Brillouin scattering, have been studied in the steady-state regime using continuous waves. However, waveguide experiments are often based on optical pump pulses, which require treatment in a dynamic framework. In this paper, we present an effective Hamiltonian formalism in the dynamic regime using optical pulses that links waveguide optomechanics and cavity optomechanics, which can be used in the classical and quantum regime including quantum noise. Based on our formalism, a closed solution for coupled-mode equation under the undepleted assumption is provided and we found that the strong coupling regime is already accessible in current Brillouin waveguides by using pulses. We further investigate several possible experiments within waveguide optomechanics, including Brillouin-based coherent transfer, Brillouin cooling, and optoacoustic entanglement.

DOI: [10.1103/PhysRevResearch.5.013010](https://doi.org/10.1103/PhysRevResearch.5.013010)

### I. INTRODUCTION

Photons are known as one of the most promising quantum information carriers in quantum communication, especially for long distances [1] but also represent a major opportunity for quantum computation [2]. However, enhancing photon-photon coupling is a challenge. Introducing optomechanical interaction is one of the possible ways to get photons more interactive and therefore mechanical systems have a profound impact on current quantum technologies. The combination of matured MEMS (microelectromechanical system) [3] technology and the diversity of mechanical systems offer flexibility for transducing, delivering, and manipulation of quantum information and moreover open new roads of exploring macroscopic quantum phenomena [4–6]. In addition to the considerable effort invested in optomechanical resonators [6,7], some research has been conducted in waveguide optomechanics [8], which may be a plausible platform for quantum networks [9] and quantum nonlinearity [10] due to its broad bandwidth and integrability into existing circuitry [11–13].

Waveguide optomechanics can rely on the interaction of optical waves with mechanical breathing modes of the transverse section of the optical waveguide or on traveling longitudinal acoustic waves or on hybrid versions of both of them. Brillouin scattering, which describes a variety of these

optoacoustic and optomechanical interactions has been experimentally investigated in detail in optical fibers and photonic integrated waveguides [14,15] and several classical coupled-mode equations [16] have been analytically developed in the classical regime to understand those phenomena. Also quantum approaches have been studied, including Hamiltonian [17] and Lagrangian treatments [18], which propose a quantum field description for optomechanical interactions in waveguides. Treating the waveguide as an array of cavities is another way towards optomechanical waveguide theories [19]. Current research on quantum regimes in an analytical way, however, focuses on steady-state behaviors and treat continuous-wave (CW) interactions. Studying dynamic processes including optical pump pulses involve challenges such as the contradiction between finite control length and the infinite expanded nature of phonons. This makes it challenging to analyze the time-dependent quantum evolution in optoacoustic processes stimulated by a pulsed pump such as Brillouin-based memory [20–22].

Compared with the well-studied zero-dimensional cavity optomechanics, where the mechanical or acoustic excitations are localized, the one-dimensional extended-waveguide systems with traveling acoustic waves present several intriguing features. Firstly, the continuous phonon spectrum in continuum optomechanical waveguides provides a remarkably large bandwidth for optomechanical interaction [23], which is an ideal platform for multimode optomechanics. Furthermore, the resonator-free structure in extended waveguide systems enables phase-preserving manipulation of the traveling waves [20,21,24]. Moreover, this one-dimensional optomechanical interaction offers new physics that was unseen in zero-dimensional cavities like polariton band structure [25,26] and topological transport [27,28].

In this paper, we formulate a framework in which backscattered Brillouin scattering in a waveguide is treated as a

\*Corresponding address: [birgit.stiller@mpl.mpg.de](mailto:birgit.stiller@mpl.mpg.de)

Published by the American Physical Society under the terms of the [Creative Commons Attribution 4.0 International license](https://creativecommons.org/licenses/by/4.0/). Further distribution of this work must maintain attribution to the author(s) and the published article's title, journal citation, and DOI. Open access publication funded by the Max Planck Society.

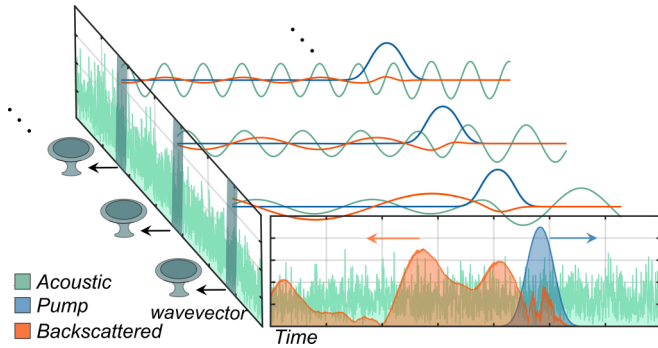


FIG. 1. Principle: The backward Brillouin interaction can be separated in different wavevector channels. In each channel, the backscattered nature contributes to a cavity-like localized interaction.

continuous cavity array in the momentum space (Fig. 1). With this framework, many techniques well developed in cavity optomechanics can be applied to the continuum optomechanical systems.

We introduce comoving coordinates that move together with the optical pump pulse, which enables a simple formulation of the pulsed dynamical regime, in which propagating optical pulses interact with traveling acoustic waves, respectively. Under the assumption of sufficiently short undepleted pump pulses, the framework maps the dynamic pulsed case in a waveguide into a cavity-like system, which greatly simplifies the treatment of different scenarios of coherent control. We find that due to the larger depletion threshold for shorter pulses, the strong coupling regime can be achieved using current platforms in the pulsed regime. With this framework, we explore several challenging problems in backward Brillouin scattering in waveguide systems, such as coherent transfer between photons and phonons, Brillouin cooling, and entanglement in Brillouin waveguide systems.

First, we analytically demonstrate that by delicately controlling the pump pulse length, coherent transfer and Brillouin cooling with high efficiency using the backward Brillouin process is possible. More specifically, we use an anti-Stokes Brillouin process in the backward regime to show that the quantum state can be transferred between photons and acoustic phonons. This transfer can be used for cooling the acoustic phonons in longer fibers with higher efficiency than those based on continuous waves [8,29]. Note that previous papers were mostly based on forwarding Brillouin scattering, which is related to transverse mechanical vibrations and presents a different operation regime [8,29]. Secondly, we analytically show that entangled pair generation is possible by using the backward Brillouin scattering Stokes process. Our evaluation suggests that these regimes can be attained by existing waveguide systems such as chalcogenide fibers and nanoscale waveguides.

The paper is organized as follows: In Sec. II we briefly summarize the conventional backward Brillouin interaction and then present the effective Hamiltonian formalism, which is the main result of this paper. In Sec. III, we investigate three challenging problems in waveguide optomechanics using our formalism: coherent transfer, Brillouin cooling, and entangled pair generation. In the last Sec. IV, we summarize our result

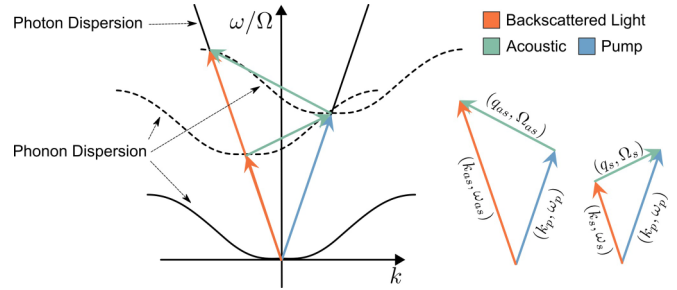


FIG. 2. The phase-matching diagram. The black corn and black curve refer to the dispersion relation of photons and acoustic phonons. The black-dotted line is the copy of the phonon dispersion relation. For the Stokes process, the phase-matching condition can only be satisfied when the pump photon emits a forward traveling phonon (the green arrow pointing to the top right corner). In contrast, the anti-Stokes process can only be stimulated when absorbing a backward traveling phonon (the green arrow pointing to the top left corner).

and discuss several open questions in waveguide optomechanics.

## II. EFFECTIVE HAMILTONIAN FORMULATION

### A. Waveguide optomechanical system

We consider an optomechanical waveguide system, which allows the guidance of both electromagnetic and acoustic waves with different wave vectors and in different spatial modes. A typical optomechanical interaction in such a waveguide system treats a mechanical oscillation with frequency  $\Omega(k)$ , a light field with optical frequency  $\omega(k)$ , and the optomechanical coupling  $g_0$ , which refers to the coupling between two photons with wave vectors  $k_S, k_p$  ( $p, q$ ) and one acoustic phonon with wave vector  $q(k)$ . The optomechanical coupling can originate from different physical processes such as electrostriction [30] and radiation pressure [31]. Considering the three-wave-mixing optomechanical coupling (usually the dominant ones), the system can be described by the Hamiltonian [17,19]

$$H = \int_{-\infty}^{+\infty} dq \hbar \omega(q) a_q^\dagger a_q + \int_{-\infty}^{+\infty} dq \hbar \Omega(q) b_q^\dagger b_q + \hbar \iint_{-\infty}^{+\infty} dq dp (g_{p,q} a_{p+q}^\dagger a_p b_q + \text{H.c.}) \quad (1)$$

where  $a_k$  and  $b_k$  are annihilation operators of the electromagnetic and mechanical modes. For the interactions within the narrow frequency band of interest, the coupling factor  $g_{p,q}$  can be approximated by a coupling constant  $g_0$ .

This Hamiltonian can be derived from combining elastic theory and Maxwell's equations by introducing an optomechanical coupling as the interaction part [17]. To treat this quantum mechanically, it is then quantized on the normal modes. The first two/three terms are the energy for photons and acoustic phonons (the free Hamiltonian part  $H_0$ ) and the last two terms are the interaction Hamiltonian  $H_I$ .

The optomechanical interactions in the waveguide are constrained by the phase-matching condition. As shown in Fig. 2, there are two points [30] where the phase-matching condition

is satisfied when the waveguide is pumped by an optical field with wavevector  $k_p$  and frequency  $\omega(k_p)$ . These two points refer to the Stokes process/anti-Stokes process with photon wavevector  $k_{s/as}$ , photon frequency  $\omega(k_{s/as})$ , phonon wavevector  $q_{s/as}$ , and phonon frequency  $\Omega(q_{s/as})$ . Since the two kinds of phonons corresponding to the Stokes and anti-Stokes process are separated in directions, we can selectively apply the Stokes process or anti-Stokes process on the directional traveling phonons by choosing the pump pulse direction.

The wave package operators are defined by integrating the wavevectors around the phase-matching points [17],

$$\begin{aligned} a_{p/as/s}(z, t) &= \frac{1}{\sqrt{2\pi}} \int_{-\infty}^{+\infty} dk \\ &\quad \times a_k e^{-i(k-k_{p/as/s})z} e^{i\omega(k_{p/as/s})t}, \\ b_{as/s}(z, t) &= \frac{1}{\sqrt{2\pi}} \int_{-\infty}^{+\infty} dq \\ &\quad \times b_q e^{-i(q-q_{s/as})z} e^{i\omega(q_{s/as})t}, \end{aligned} \quad (2)$$

where the first equation corresponds to the optical waves and the second equation to the acoustic wave. The fiber is placed on the  $z$  axis in the laboratory frame and the pump wave is assumed to be propagating along the positive  $z$  axis. It can be verified that the wave package operators and the corresponding Hermite conjugates are well-defined quantum operators that preserve the commutation relations. Utilizing the wave package operators, the interaction part  $H_I$  can be written as the products in both Stokes process ( $H_{I,S}$ ) and the anti-Stokes ( $H_{I,AS}$ ) process,

$$\begin{aligned} H_{I,S} &= g_0 \hbar \int_{-\infty}^{+\infty} dz a_p^\dagger(z) a_s(z) b_s(z) + \text{H.c.}, \\ H_{I,AS} &= g_0 \hbar \int_{-\infty}^{+\infty} dz a_p(z) a_{as}^\dagger(z) b_{as}(z) + \text{H.c.} \end{aligned} \quad (3)$$

From the Heisenberg equation of the optomechanical Hamiltonian, we can derive the approximated motion equation for  $a_{p/s/as}(z, t)$  and  $b_{as/s}(z, t)$ , which are the coupled-mode equations for the stimulated Brillouin scattering process. Here, we write the coupled-mode equations for the backward Brillouin process, which will be the important process throughout this paper.

For the Stokes process, the equations are

$$\begin{aligned} \partial_t a_p + c_g \partial_z a_p &= -ig_0 a_s b_s - \gamma/2 a_p, \\ \partial_t a_s - c_g \partial_z a_s &= -ig_0 a_p b_s^\dagger - \gamma/2 a_s, \\ \partial_t b_s + u_g \partial_z b_s &= -ig_0 a_p a_s^\dagger - \Gamma/2 b_s + \sqrt{\Gamma} \xi. \end{aligned} \quad (4)$$

For the anti-Stokes process, the equations are

$$\begin{aligned} \partial_t a_p + c_g \partial_z a_p &= -ig_0 a_{as} b_{as}^\dagger - \gamma/2 a_p, \\ \partial_t a_{as} - c_g \partial_z a_{as} &= -ig_0 a_p b_{as} - \gamma/2 a_{as}, \\ \partial_t b_{as} - u_g \partial_z b_{as} &= -ig_0 a_p^\dagger b_{as} - \Gamma/2 b_{as} + \sqrt{\Gamma} \xi. \end{aligned} \quad (5)$$

The  $a_p$ ,  $a_s$ ,  $a_{as}$  refer to the optical wave packets for the pump wave, Stokes wave, and the anti-Stokes wave respectively. The  $b_s$  and  $b_{as}$  refer to the acoustic wave packets related to the two processes. The optical excitations and the acoustic

excitations travel in the fiber in different group velocities described by  $c_g$ ,  $u_g$  and suffer a dissipation rate with  $\gamma$ ,  $\Gamma$ . Since the acoustic excitations travel much slower than the optical ones, therefore we can omit this effect by setting  $u_g = 0$  in the following discussion. The thermal noise of the acoustic field is taken into consideration with the Langevin term  $\sqrt{\Gamma} \xi$ .  $\xi = \xi(z, t)$  obeys the relations

$$\begin{aligned} \langle \xi(z_1, t_1) \xi^\dagger(z_2, t_2) \rangle &= n_{th} \delta(z_1 - z_2, t_1 - t_2), \\ [\xi(z_1, t_1), \xi^\dagger(z_2, t_2)] &= \delta(z_1 - z_2, t_1 - t_2). \end{aligned} \quad (6)$$

$n_{th}$  is the averaged thermal phonon number at the given temperature

$$n_{th} = \frac{1}{e^{\epsilon_p/k_B T_E} - 1}, \quad (7)$$

where  $\epsilon_p$  is the energy of a single phonon,  $k_B$  is the Boltzmann constant, and  $T_E$  is the temperature of the environment.

The coupled-mode equation above can be used for numerical simulations. However, finding an analytical solution for the dynamical cases of optical and acoustic pulses and investigating analytically quantum phenomena are both not straightforward with this set of equations. In the following sections, we will show that the coupled mode equations can be exactly solved under the undepleted assumption.

## B. The undepleted assumption

In the following discussions, we consider the undepleted case. The undepleted assumption refers to the condition where the waveform function of the pump light  $a_p(z, t)$  remains unchanged during the scattering process. This assumption is valid for quantum Brillouin experiments, where the amplitude of the quantum-level acoustic field and backscattered field like Stokes and anti-Stokes wave are too small to deplete the pump significantly.

Defining

$$g(z, t) = g_0 \langle a_p(z, t) \rangle; \quad (8)$$

since the pump waveform  $a_p(z, t)$  remained unchanged during the propagation, the  $g(z, t)$  would remained unchanged too,

$$a_p(z, t) = a_p(0, t - z/c_g) \iff g(z, t) = g(0, t - z/c_g). \quad (9)$$

Under the undepleted assumption, the first equation in the coupled mode equations, which refers to the pump dynamics, can therefore be omitted. For example, the coupled mode equation for the Stokes process can be linearized as

$$\begin{aligned} \partial_t a_s - c_g \partial_z a_s &= -ig b_s^\dagger - \gamma/2 a_s, \\ \partial_t b_s &= -iga_s^\dagger - \Gamma/2 b_s + \sqrt{\Gamma} \xi. \end{aligned} \quad (10)$$

Under the undepleted assumption, the equations are now linearized. The effective coupling strength  $g(z, t)$  describes the coupling between the acoustic and optical fields, which is tunable by changing the pump power. This tunable coupling strength enables us to control the acoustic phonons and photons traveling in the waveguide system coherently. Furthermore, as discussed later, we will show that the strong coupling conditions  $g > \Gamma$  are possible by applying strong short pump pulses under the pulse Brillouin threshold. The

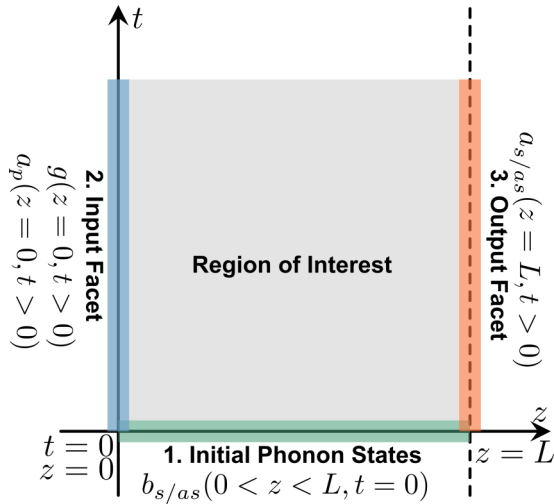


FIG. 3. The region of interest in backscattered Brillouin scattering problems. Besides noise, three boundary conditions need to be specified for both Stokes process and the anti-Stokes process so that the coupled mode equation can be mathematically complete: (1) the initial phonon states at  $t = 0$ . (2) the input pump waveform at  $z = 0$ . (3) the input backscattered waveform at  $z = L$ .

detailed strong coupling condition and the pulsed threshold are discussed later in Sec. II F 4.

### C. Boundary value problem

Considering a fiber of length  $L$ , we assume that there is no light in the fiber at  $t = 0$  and all the light waves are input at either the end at  $z = 0$  or the end at  $z = L$  of the fiber at  $t > 0$ . To determine the whole evolution of all wave packets functions in the fiber at  $t > 0$ ,  $0 < z < L$ , we need to know (1) the initial acoustic states  $b_{s/as}(z, t = 0)$ ; (2) the input pump waveform  $a_p(z = 0, t)$ , when linearized, this terms can be fully described by  $g(z = 0, t)$ ; (3) the input backscattered waveform  $a_{s/as}(z = L, t)$ ; and (4) the detailed form of the noise function  $\xi(z, t)$ . If we only care about the statistical result, the detailed form of the noise function is not needed.

The scattering process can be described in a space-time diagram like the following, in this space-time diagram, the above requirements all appear at the boundaries, as shown in Fig. 3.

### D. Exact solution under undepleted assumption

By defining the coordinates transformation

$$\eta = t - z/c_g, \quad \tau = t, \quad (11)$$

the distribution coupling strength  $g(z, t)$  can be directly related to the boundary conditions  $g(z = 0, t) = g_0(a_p(z = 0, t))$ ,

$$g(z, t) = g(0, t - z/c_g) = g(\eta). \quad (12)$$

Take the Stokes process as an example, the linearized coupled mode equations for the Stokes process can be further written

as (the derivation is detailed in Appendix A)

$$\begin{aligned} (\partial_\tau + 2\partial_\eta)a_s &= -igb_s^\dagger - \gamma/2 a_s, \\ (\partial_\tau + \partial_\eta)b_s^\dagger &= iga_s - \Gamma/2 b_s^\dagger + \sqrt{\Gamma}\xi^\dagger. \end{aligned} \quad (13)$$

Since  $g$  only depends on  $\eta$ , the variables in the above equation can be separated by performing a Fourier transformation on variable  $\tau$ ,

$$\begin{aligned} \tilde{a}_s(\Delta, \eta) &= \frac{c_g}{L} \int_0^{L/c_g} d\tau a_s(\tau, \eta) e^{-ic_g\Delta\tau}, \\ \tilde{b}_s^\dagger(\Delta, \eta) &= \frac{c_g}{L} \int_0^{L/c_g} d\tau b_s^\dagger(\tau, \eta) e^{-ic_g\Delta\tau}, \\ \tilde{\xi}^\dagger(\Delta, \eta) &= \frac{c_g}{L} \int_0^{L/c_g} d\tau \xi^\dagger(\tau, \eta) e^{-ic_g\Delta\tau}. \end{aligned} \quad (14)$$

Then the equation can be written as the following Langevin form:

$$\partial_\eta \begin{pmatrix} \tilde{a}_s \\ \tilde{b}_s^\dagger \end{pmatrix} = \begin{pmatrix} -\frac{\gamma+2ic_g\Delta}{4} & -\frac{ig}{2} \\ ig & -\frac{2ic_g\Delta+\Gamma}{2} \end{pmatrix} \begin{pmatrix} \tilde{a}_s \\ \tilde{b}_s^\dagger \end{pmatrix} + \begin{pmatrix} 0 \\ \sqrt{\Gamma}\tilde{\xi}^\dagger \end{pmatrix}. \quad (15)$$

It has to be noted that the closed solution for anti-Stokes process can be obtained in the same way. For the anti-Stokes process, a similar Langevin form can be obtained,

$$\partial_\eta \begin{pmatrix} \tilde{a}_{as} \\ \tilde{b}_{as} \end{pmatrix} = \begin{pmatrix} -\frac{\gamma+2ic_g\Delta}{4} & -\frac{ig}{2} \\ -ig & -\frac{2ic_g\Delta+\Gamma}{2} \end{pmatrix} \begin{pmatrix} \tilde{a}_{as} \\ \tilde{b}_{as} \end{pmatrix} + \begin{pmatrix} 0 \\ \sqrt{\Gamma}\tilde{\xi} \end{pmatrix}. \quad (16)$$

The matrices in the above equations can be made Hermitian by variable substitution:  $\tilde{A} = \frac{\sqrt{2}}{2}\tilde{a}$ ,  $\tilde{B} = \tilde{b}$ . The initial phonon states and backward laser injections (Stokes and anti-Stokes part) are included in the initial conditions at  $\eta = 0$ . The above equations, describing the evolution of each Fourier component  $\Delta$ , are similar to the Langevin equation in optomechanics cavities. The only difference is the time evolution in optomechanics cavities is now replaced by the  $\eta$  evolution on a copropagating framework. Each Fourier component with off-resonance variable  $\Delta$  can be written with the corresponding equation of  $\eta$  evolution, and the equations are independent of each other. This separability indicates a new viewpoint of waveguide optomechanics that by separating the interactions to different frequency/wavevector channels, cavity-like behavior can be recovered. The detail of this similarity is depicted in Fig. 1 and is discussed in detail in Sec. II E.

The Langevin equations above are exactly solvable, which means that once we obtained the boundary conditions at  $\eta = 0$ , then the exact solutions can be obtained in the solvable region as shown in Fig. 4. As with the conventional Langevin equations, a Green's function, also called the time-evolution operator, can be introduced to obtain the exact solution. The Langevin equation in a general matrix form reads

$$\frac{d\vec{M}(\eta)}{d\eta} = \mathbf{P}(\eta)\vec{M}(\eta) + \vec{R}(\eta). \quad (17)$$

We now introduce the Green's function

$$\mathbf{G}(\eta_2, \eta_1) = \mathcal{T} \left\{ \exp \int_{\eta_1}^{\eta_2} d\nu \mathbf{P}(\nu) \right\}. \quad (18)$$

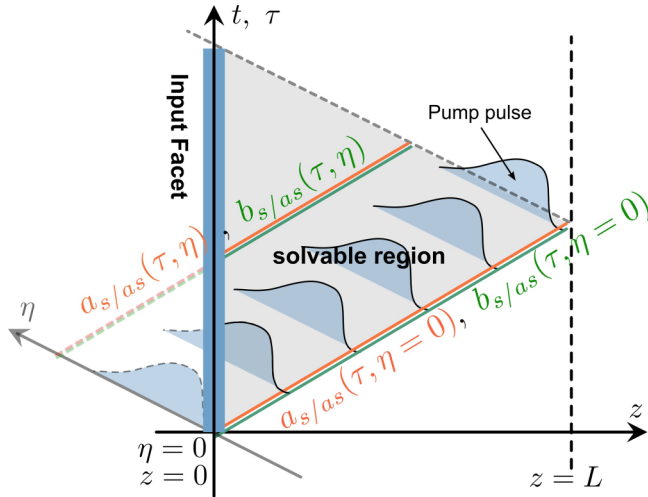


FIG. 4. The exact solvable region. Under the undepleted assumptions, separation of variables could be applied to the coupled mode equation after variable transformation  $(z, t) \rightarrow (\tau, \eta)$ . In this case, the exact solution of the scattering process can be obtained in the gray triangle region shown in this figure. To obtain the exact solution in this region, two boundary conditions are needed: (1) the phonon and backscattered waveform at  $\eta = 0$ ,  $a_{s/as}(\tau, \eta = 0)$ ,  $b_{s/as}(\tau, \eta = 0)$ . (2) The coupling strength at every  $\eta$ ,  $g(\eta) = g_0 a_p(0, t = \eta)$ .

The  $\mathcal{T}\{\dots\}$  is the time-ordering operator to ensures the exponential is time ordered, which in context means  $\eta$  ordered: any product of  $\mathbf{P}(v)$  that occurs in the expansion of the exponential must be ordered such that the value of  $v$  is increasing from right to left of the product. The solution can be written as

$$\vec{M}(\eta) = \mathbf{G}(\eta, 0)\vec{M}(0) + \int_0^\eta dv \mathbf{G}(\eta, v)\vec{R}(v). \quad (19)$$

As shown in Eq. (8), the pump laser can be fully described as a modification of the effective coupling. Under the undepleted assumption, the pump pulse travels along the fiber without changing its waveform. Therefore all points on the fiber experience the same effective coupling waveform. In our formalism [Eqs. (15) and (16)], this can be fully described by  $g(z, t) = g(0, t - z/c_g) = g_0 \langle a_p(0, t - z/c_g) \rangle$  using the pulse waveform at the input port. Therefore we can claim that all undepleted situation has been solved.

To demonstrate the formalism developed here, we consider a rectangular pump shape, where

$$g(\eta) = g\Theta(\eta)\Theta(T - \eta). \quad (20)$$

In this case, the solution can be written as (when  $t \leq T$ )

$$\vec{M}(\eta) = \mathbf{G}(\eta)\vec{M}(0) + \int_0^\eta dv \mathbf{G}(\eta - v)\vec{R}(v) \quad (21)$$

with

$$\mathbf{G}(\eta) = \exp(\mathbf{P}\eta). \quad (22)$$

### E. Physics interpretation: Comoving conditions

In this section, we show that the physics behind the variable-separated equations [Eqs. (15) and (16)] reveals a similarity between waveguide systems and cavity systems:

The interaction can be separated into cavity-like interactions in different wavevector channels.

We choose the Stokes interaction as an example. Consider the initial state at  $t = 0$ , which can be written as

$$\begin{aligned} a_s(z, t = 0) &= \sum_k A_k e^{ikz} \\ b_s^\dagger(z, t = 0) &= \sum_k B_k^\dagger e^{ikz}. \end{aligned} \quad (23)$$

When the noise and dissipation are omitted and there is no pump light in the waveguide at  $t = 0$ , this initial state leads to a solution at  $z = c_g t$  (which corresponds to  $\eta = 0$  in the  $\eta - \tau$  coordinates) and yields

$$\begin{aligned} a_s(z = c_g t, t) &= a_s(z + c_g t, 0) = \sum_k A_k e^{2ikc_g t}, \\ b_s^\dagger(z = c_g t, t) &= b_s^\dagger(z, 0) = \sum_k B_k^\dagger e^{ikc_g t}. \end{aligned} \quad (24)$$

Applying Eq. (14) results in

$$\begin{aligned} a_s(\tau, \eta = 0) &= \sum_\Delta \tilde{a}_s(\Delta, \eta = 0) e^{ic_g \Delta \tau}, \\ b_s^\dagger(\tau, \eta = 0) &= \sum_\Delta \tilde{b}_s^\dagger(\Delta, \eta = 0) e^{ic_g \Delta \tau}, \end{aligned} \quad (25)$$

with

$$\begin{aligned} \tilde{a}_s(\Delta, \eta = 0) &= A_{\Delta/2}, \\ \tilde{b}_s^\dagger(\Delta, \eta = 0) &= B_{\Delta}^\dagger. \end{aligned} \quad (26)$$

From Eq. (26) we can see that the physics interpretation of  $\tilde{a}_s(\Delta, \eta)$  and  $\tilde{b}_s^\dagger(\Delta, \eta)$  in Eq. (14) corresponds to the amplitude in the wavevector picture. Therefore, the separation of the original coupled mode equation Eq. (4) [Eq. (5)] into Eq. (15) [Eq. (16)] indicates the interaction in waveguides can be separated into cavity-like interactions in different wavevector channels, by only pairing each optical wave components with the acoustic wave components with twice the wavevector. One of the main differences between optomechanical waveguides and optomechanical cavities is the Hilbert space. In optomechanical resonators, the phonon states and the photon states are discrete. In waveguides, the phonon and photon spectrum is continuous. Therefore, we have to consider a spectrum-dependent interaction in the optomechanical waveguide. In our case, the interaction is only significant near the phase matching point, and  $\Delta$  here is the wavevector deviation from the phase matching point.

Furthermore, for a special initial plane wave initial state as

$$\begin{aligned} a_s(z, t = 0) &= A_{k_0/2} e^{ik_0 z/2}, \\ b_s^\dagger(z, t = 0) &= B_{k_0}^\dagger e^{ik_0 z}, \end{aligned} \quad (27)$$

only  $\Delta = k_0$  would lead to nonzero  $\tilde{a}_s$  and  $\tilde{b}_s^\dagger$ . Therefore, for every  $\eta$ , we have

$$\begin{aligned} \forall \delta \tau > 0, \\ a_s(\eta, \tau + \delta \tau) &= a_s(\eta, \tau) e^{ic_g k_0 \delta \tau}, \\ b_s^\dagger(\eta, \tau + \delta \tau) &= b_s^\dagger(\eta, \tau) e^{ic_g k_0 \delta \tau}. \end{aligned} \quad (28)$$

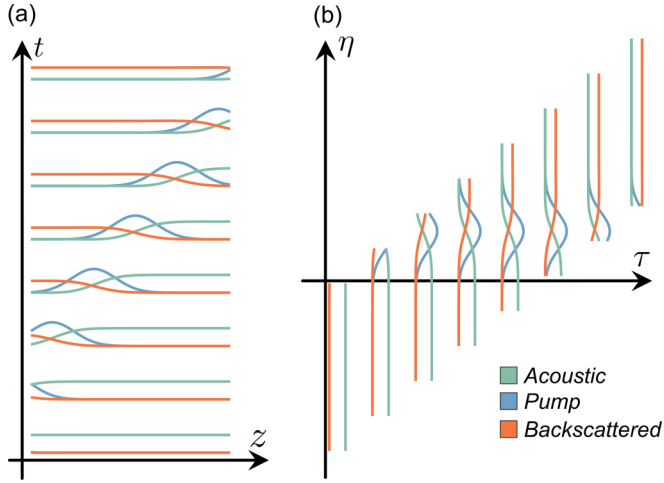


FIG. 5. The physics behind the solutions: Comoving conditions. If we omit the noise and depletion, a comoving condition Eq. (28) can be derived once the plane-wave-like initial conditions in Eq. (27) is satisfied. (a) In the  $z - t$  coordinates, or the laboratory frame, both the backscattered light and the acoustic waveform (in terms of amplitudes) are comoving with the pump. (b) In the  $\eta - \tau$  coordinates, all the waveforms are constant along the  $\tau$  axis. The phase factor is omitted in both (a) and (b). This comoving condition means that in the comoving frame of the pump pulse, the waveform of both acoustic and backscattered waves will remain unchanged except for a phase factor  $e^{i\Delta z}$ . This makes the nonlocalized interaction process in the waveguides similar to the localized interaction in the optical cavities, and this is the physics reason why we can treat waveguides using similar methods in the cavities.

Converting this back to the  $z - t$  laboratory frame, we have a nontrivial observation

$$\begin{aligned} \forall \delta t > 0, \\ a_s(z + c_g \delta t, t + \delta t) &= a_s(z, t) e^{i c_g k_0 \delta t}, \\ b_s^\dagger(z + c_g \delta t, t + \delta t) &= b_s^\dagger(z, t) e^{i c_g k_0 \delta t}. \end{aligned} \quad (29)$$

This condition means that the waveform of both the acoustic field and the backscattered optical field remain unchanged in the comoving frame along with the propagating pump except for an additional phase factor  $e^{i c_g \tau}$ , as shown in Fig. 5. This comoving frame in a special case  $\Delta = 0$  is also discussed in Ref. [32]. This turns the nonlocalized interaction in waveguides into a cavity-like localized interaction in the comoving frame. Figure 1 depicts the consequence of this assumption: The whole scattering process in the waveguide can be separated into different frequency channels. In each of the channels, translational invariances hold, and that enables us to build a mathematical framework to connect the waveguide optomechanics and the cavity optomechanics.

This result indicates that the pump pulse length can be used to control the evolution time for phonons and photons in waveguides. Exactly controlling the interaction time enables us to control the optoacoustic interaction coherently, which makes the dynamic regime more interesting for coherent control applications, in contrast to the steady-state regime. In the following sections, we will discuss some predictions derived from this formalism.

## F. Waveguide optomechanics in the perspective of cavity optomechanics: With backward Brillouin scattering as an example

### 1. The beam-splitter-like and down-conversion-like interaction

The Brillouin interaction Hamiltonian is described in Eq. (3). In the case of linearizing the interaction using undepleted pump assumption, different phase matching conditions lead to different effective Hamiltonians. The interaction Stokes Hamiltonian  $H_{I,S}$  describes a down-conversion-like process between the Stokes photons and the phonons, which corresponds to the blue-detuned regime in cavity optomechanics. The anti-Stokes part  $H_{I,AS}$  describes a beam-splitter-like process, which is similar to the red-detuned regime in cavity optomechanics [6].

In terms of cavity optomechanics, the beam-splitter-like interaction (the anti-Stokes process here) describes a state transfer between the anti-Stokes photons and phonons [33]. Such conversion process is the Rabi oscillation and can be used to achieve coherent transfer. The area dependency in Brillouin memory is exactly the result of area dependency in Rabi oscillation [34], as explained later.

As for this down-conversion-like interaction, i.e., the Stokes process is a parametric amplification process [4], the scattered Stokes field can grow much more quickly than the anti-Stokes field when the pump power is high enough, which causes asymmetric Stokes and anti-Stokes sidebands.

### 2. The Brillouin gain and the strong coupling regime

In this section, we relate our approach to commonly used experimental parameters in backward stimulated Brillouin scattering (SBS) experiments.

In SBS, the Stokes process is dominant. We consider the steady state in which both  $\frac{\partial a_s}{\partial t}$  and  $\frac{\partial b}{\partial t}$  equal to zero in Eq. (4) and introduce the acoustic dissipation rate  $\Gamma$ . Then we get

$$\frac{\partial}{\partial z} (a_s^\dagger a_s) = -\frac{4g_0^2 a_p^\dagger a_p}{\Gamma c_g} a_s^\dagger a_s. \quad (30)$$

In SBS generated by a continuous pump, it holds  $\frac{\partial}{\partial z} (a_s^\dagger a_s) = -GPa_s^\dagger a_s$ . The  $G$  refers to the Brillouin gain whose unit is  $[m^{-1}W^{-1}]$  and the  $P$  refers to the pump power, whose unit is  $[W]$ . Therefore the effective gain we introduce can be obtained from the pump power directly [16]

$$|g| = \sqrt{\frac{GP\Gamma c_g}{4}}. \quad (31)$$

A dimensionless effective coupling ratio  $|g|/\Gamma$  can be introduced by utilizing Eq. (31). Coherent control is only possible when the effective coupling ratio is larger than one,

$$\frac{|g|}{\Gamma} = \sqrt{\frac{GPc_g}{4\Gamma}} > 1. \quad (32)$$

Generally the strong coupling regime in cavity optomechanics denotes that the intensity of the optomechanical coupling strength exceeds the dissipation rates of the optical and mechanical modes [6]. For the backward Brillouin scattering in typical waveguides, as the acoustic dissipation generally exceeds the optical dissipation, the system enters into the strong coupling regime when the coupling strength becomes larger

than the acoustic dissipation rate, i.e.,  $|g| > \Gamma$ . As shown in Eq. (16), the Rabi period is inverse proportional to  $|g|$ . Therefore the strong coupling regime here can be interpreted as a longer phonon lifetime than the Rabi period.

In reported waveguide systems, when pump pulse power is 1W, a coupling ratio as high as  $|g|/\Gamma = 8.3$  can be achieved in the integrated chalcogenide waveguides [35]. Other potential platform to demonstrate the predictions in this paper are nanowaveguides [36,37] where radiation-pressure-based Brillouin gain enhancement was proven by carefully engineering the geometry and fiber systems, such as chalcogenide and photonic crystal fibers with reported large Brillouin gain coefficients [38,39]. Moreover, due to the reduced phonon dissipation and enhanced Brillouin gain at low temperatures [40,41], demonstration of this strong coupling regime could be possible on more platforms in a cryogenic environment.

### 3. Area dependency

SBS can be used to coherently transfer information from the optical domain to acoustic waves. This concept has been experimentally shown as Brillouin memory [20,21]. In Brillouin memory, the write/read efficiency attains a maximum when the effective coupling area  $\Theta(T) = \int_0^T dt g_0 \sqrt{|a_p^\dagger(t)a_p(t)|}$  satisfies the following area dependency equation [20,21,34,42]:

$$\Theta = (2n + 1) \frac{\sqrt{2}\pi}{2} \quad (n \in \mathbb{Z}). \quad (33)$$

This result can be recovered by our formalism in a straightforward way. The readout process in Brillouin memory experiment is the anti-Stokes process, which is described by Eq. (16). We consider the perfect phase-matching case where  $\Delta = 0$  and omitting the dissipation  $\Gamma$ ,  $\gamma = 0$  as in Ref. [34]. If the system is driven by a rectangular pump pulse as described in Eq. (20), the matrix elements of the propagator in Eq. (22) that describes photon-phonon transfer reads

$$\begin{aligned} \frac{1}{2} |\mathbf{G}_{21}(\eta > T)| &= |\mathbf{G}_{12}(\eta > T)| \\ &= \left| \sin \left( \frac{\sqrt{2}}{2} gT \right) \right| \\ &= \left| \sin \left( \frac{\sqrt{2}}{2} \Theta(T) \right) \right|. \end{aligned} \quad (34)$$

The  $|\mathbf{G}_{21}|$  and  $|\mathbf{G}_{12}|$  attains maxima if and only if the area dependency in Eq. (33) is satisfied.

### 4. The undepleted condition

Our formalism is built based on the undepleted pump approximation. When the pump power is strong enough and the pulse length is sufficiently long, the pump power might be significantly depleted by the Stokes process. The anti-Stokes process is much weaker than the Stokes process, and therefore it is enough for us to only consider the Stokes process.

For a short pulse length in the Stokes process, the second term in the solution of Langevin equation (21) can be omitted, since the first term in Stokes process described by

Eq. (15) has an exponential growing term, which significantly surpasses the second term [32]. From a physical point of view, the Stokes process is a stimulated amplification process. The amplification of the initial state fluctuation is going to be much greater than the additional noise added during the evolutionary process,

$$\langle \tilde{a}_S^\dagger(\Delta, \eta) \tilde{a}_S(\Delta, \eta) \rangle \approx |\mathbf{G}_{12}(\Delta, \eta)|^2 n_{th}. \quad (35)$$

The  $n_{th}$  is the average thermal phonon number,  $n_{th} \approx k_B T_E / (\hbar \Omega)$ . The undepleted condition requires that the Stokes power is much smaller than the pump power,  $I_S \ll I_P$ . For a rectangular pulse with pulse length  $T$  as defined in Eq. (20), the requirement can then be simplified to

$$\frac{\sqrt{2}}{2} gT \ll \frac{1}{4} \ln \frac{32\pi^2 I_P \Omega^2}{\Gamma c_g k_B^2 T_E^2 \omega^2}. \quad (36)$$

The detailed derivation can be found in Appendix B. The left-hand side of Eq. (36) refers to the Rabi area, which equals to  $2\pi$  for a complete Rabi period. As an example, for a chalcogenide waveguide [35] pumped by 1W at room temperature, the right-hand side of Eq. (36) is  $10.27 > 2\pi$ , which means that for those pulses within the first Rabi period, the undepleted condition holds. This result also implies that increasing the pump power while decreasing the pulse length makes the undepleted assumption more robust while keeping the effective coupling area unchanged. The significant increase of depletion threshold using short pulses, which is also the Brillouin threshold, is also predicted and verified experimentally in Ref. [32].

## III. APPLICATIONS OF COHERENT CONTROL

In this section, we will use the techniques developed in the previous section to discuss coherent transfer, cooling, and entangled pair generation in backward Brillouin scattering. For simplicity, we only consider the case where the waveform of the pump light is a rectangular wave, although the method we proposed earlier is not only applicable to rectangular waves.

### A. Coherent transfer

The most critical task of optomechanical systems is the manipulation of phonon states. How to store information into phonons, read out the phonon states, and convert them into measurable physical quantities therefore becomes an important issue. Coherent transfer has been demonstrated in cavity optomechanics [33,43,44], here we show that a similar formalism can be applied to waveguide optomechanics in the pulsed regime.

The main idea to implement phonon readout is to use the anti-Stokes process: The beam-splitter-like Hamiltonian of the anti-Stokes process describes a Rabi oscillation between photons and phonons. Thus, coherent transfer between photons and phonons is possible by controlling the Rabi oscillation. The coherent transfer process can be illustrated using the space-time diagram in Fig. 6. The classical Brillouin coherent readout has been demonstrated experimentally on photonic chips [21]. As shown in the previous sections, due to the lack of resonating structures in optomechanical waveguides,

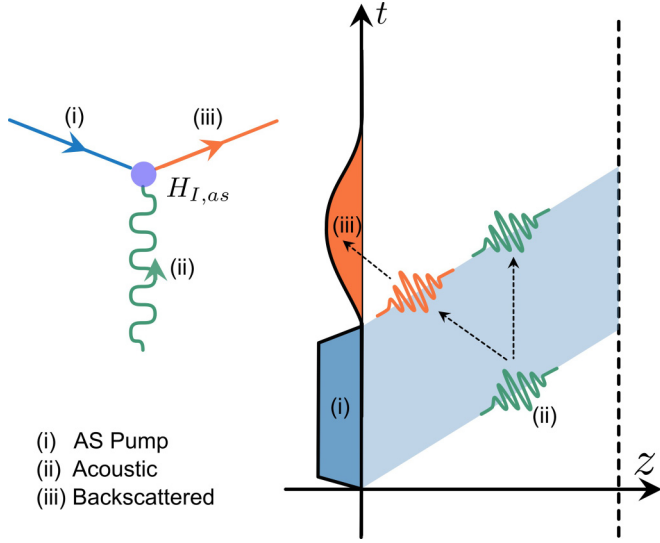


FIG. 6. Illustration of the coherent transfer and cooling process. The anti-Stokes interaction  $H_{I,AS}$  describes a Rabi-oscillation between the anti-Stokes photons and phonons. Thus a  $\pi/2$  Rabi pulse can be used to transfer the phonon into photons coherently (vice versa), and once the phonons are transferred into photons, cooling is attained.

we must consider the entire continuous phonon spectrum to derive the spectrum dependent coherent-transfer efficiency.

The spectrum dependent read out efficiency  $\beta(\Delta, \eta)$  is defined as the following: Assume that the phonon number at wavevector  $\Delta$  at the beginning of the readout process  $t = 0$  is  $N_{b,c}(\Delta, \eta) = \langle \tilde{b}_{as}^\dagger(\Delta, 0) \tilde{b}_{as}(\Delta, 0) \rangle$ , which is the coherent part we want to readout. After applying the coherent readout process, the phonons will be converted into photons, because of the existence of thermal noise, such readout process is only partially coherent,  $N_A(\Delta, \eta) = N_{a,c}(\Delta, \eta) + N_{a,n}(\Delta, \eta)$ , where the  $N_{a,c}(\Delta, \eta) = \langle \tilde{a}_{as}(\Delta, \eta)^\dagger \tilde{a}_{as}(\Delta, \eta) \rangle$  is the coherent part and  $N_{a,n}(\Delta, \eta) = \langle \tilde{a}_{as}(\Delta, \eta)^\dagger \tilde{a}_{as}(\Delta, \eta) \rangle - N_{a,c}(\Delta, \eta)$  is the noise part.

Therefore, the readout efficiency could be divided into two parts, i.e., the coherent readout efficiency and the thermal noise term. The coherent readout efficiency corresponding to the coherent transfer from phonons to photons can be given by

$$\beta_C(\Delta, \eta) = \frac{N_{a,c}(\Delta, \eta)}{N_{b,c}}, \quad (37)$$

and the thermal noise-induced part can be expressed as

$$\beta_N(\Delta, \eta) = \frac{N_{a,n}(\Delta, \eta)}{n_{th}}, \quad (38)$$

where we assume that the acoustic dissipation rate  $\Gamma$  is much larger than the optical dissipation rate  $\gamma$ . Thus the total output photon number after the readout process can be given by

$$N_A(\Delta, \eta) = \beta_C(\Delta, \eta)N_{b,c} + \beta_N(\Delta, \eta)n_{th}, \quad (39)$$

where the first term corresponds to the coherently transferred photons while the second term belongs to the noise-induced photons.

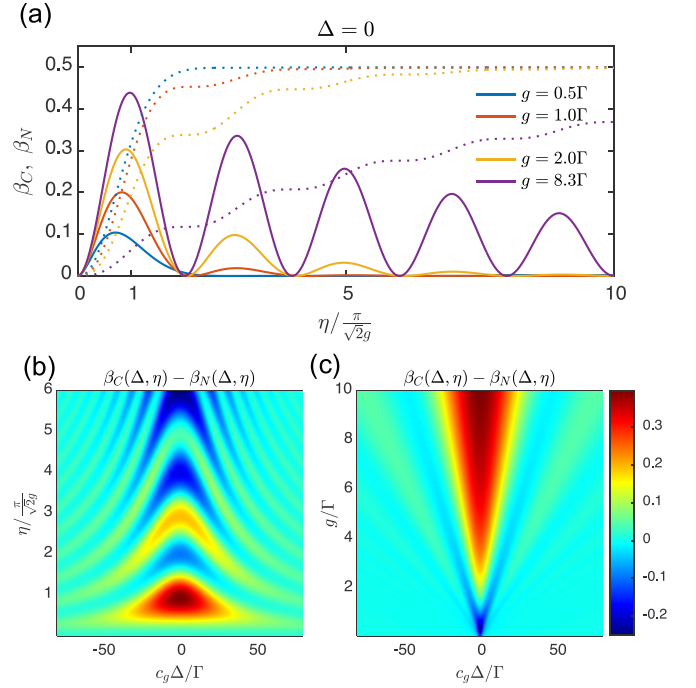


FIG. 7. The Brillouin coherent transfer. (a) Shows how the coherent transfer coefficient  $\beta_C$  (solid line) and the noise coefficient  $\beta_N$  (dotted line) changes as the pulse length increases. As the pump length increases, the coherent part oscillates, and the body of the phonon is dominated by the noise part when the pulse length is long. (b) The transfer efficiency difference  $\beta_C - \beta_N$  was calculated using  $g = 8.3\Gamma$  (Chalcogenide chip [35]) with pump power equals 1 W. A clear oscillating behavior due to the Rabi nature can be seen. Optimal coherent transfer can be attained when the difference between  $\beta_C$  and  $\beta_N$  is largest. (c) The transfer efficiency difference  $\beta_C - \beta_N$  at different coupling strengths, when pump length equals the  $\pi/2$  Rabi pulse  $t = \pi/\sqrt{2}g$ . As the coupling ratio  $g/\Gamma$  increases, both the transfer efficiency and the effective transfer spectrum bandwidth will increase.

Figure 7(a) presents how the coherent part  $\beta_C$  and the noise part  $\beta_N$  changes as pulse length increases, at the perfect phase-matched case  $\Delta = 0$ . Due to the beam-splitter nature of the anti-Stokes process, the coherent part oscillates while the maximum is attained at the first peak due to the combination of Rabi-like oscillation and thermal dissipation. However, the incoherent noise term accumulates and dominates later. The result shows that effective coherent transfer can only be possible when the  $\pi/2$  Rabi pulse is shorter compared to the phonon lifetime.

Solving the Langevin equation using propagator matrix  $\mathbf{G}$  in Eq. (22), the readout photon is

$$\begin{aligned} \tilde{a}_{as}(\Delta, \eta) = & \mathbf{G}_{11}(\Delta, \eta)\tilde{a}_{as}(\Delta, 0) + \mathbf{G}_{12}(\Delta, \eta)\tilde{b}_{as}(\Delta, 0) \\ & + \sqrt{\Gamma} \int_0^\eta d\nu \mathbf{G}_{12}(\Delta, \eta - \nu) \tilde{\xi}(\Delta, \nu). \end{aligned} \quad (40)$$

Since we consider that there is no anti-Stokes light in the waveguide at the  $t = 0$  moment in the readout process,  $\tilde{a}_{as}(\Delta, 0) = 0$ . The spectrum dependent readout efficiency



$\beta_{C,N}(\Delta, \eta)$  for a rectangular pump pulse with length  $\eta$  reads

$$\begin{aligned}\beta_C(\Delta, \eta) &= |\mathbf{G}_{12}(\Delta, \eta)|^2 \\ \beta_N(\Delta, \eta) &= \Gamma \int_0^\eta d\nu |\mathbf{G}_{12}(\Delta, \nu)|^2,\end{aligned}\quad (41)$$

where

$$\mathbf{G}_{12} = -ie^{-\frac{1}{4}\Gamma_{e,as}^*\eta - ic_g\Delta\eta} \frac{g}{\sqrt{2}g_{e,as}} \sin\left(\frac{\sqrt{2}}{2}g_{e,as}\eta\right). \quad (42)$$

The resonance-modified effective coupling strength  $g_e$  and the effective acoustic dissipation is defined as

$$\begin{aligned}g_{e,as} &= \sqrt{g^2 - (\Gamma + ic_g\Delta)^2/8}, \\ \Gamma_{e,as} &= \Gamma + ic_g\Delta.\end{aligned}\quad (43)$$

The detailed derivation of  $\mathbf{G}_{12}$  can be found in Appendix C.

We present the numeric result for  $\beta_C(\Delta, \eta) - \beta_N(\Delta, \eta)$  in Figs. 7(b) and 7(c) to illustrate the competing effects between the coherent part  $\beta_C$  and the noise-induced part  $\beta_N$  of the phonon-photon transfer efficiency. As shown in Fig. 7(b), the readout efficiency oscillates as the pulse length increases, which agrees with the area dependency law in Brillouin memory [42]. As the pulse length increases, noise phonon dominates and the coherent readout becomes inefficient. The optimal coherent readout can be achieved when

$$\eta \approx \frac{\pi}{\sqrt{2}g}. \quad (44)$$

This is exactly the  $\pi/2$  Rabi pulse length slightly modified due to the dissipation effect. Figure 7(c) shows the readout efficiency difference  $\beta_C - \beta_N$  calculated at  $\eta = \pi/(\sqrt{2}g)$ , which is the  $\pi/2$  Rabi pulse length. It can be seen that both larger readout bandwidth and higher maximum readout efficiency can be achieved by increasing the coupling strength  $g$ . Figures 7(a) and 7(b) show oscillating behaviors along the wave vector  $\Delta$ , which is related to the higher harmonics components in the Fourier transformation of rectangular waves.

Moreover, as depicted in Eq. (41) and Figs. 7(b) and 7(c), we can see that the transferred anti-Stokes wave includes photons with a continuous band of accessible states without the requirements of optical or acoustic resonators. Thus compared with the state transfer in cavity optomechanics [33,43,44], which operates with single optical and mechanical modes, the state transfer generated by Brillouin interaction in waveguides has a broader bandwidth, which is important for applications in photonic information processing, quantum computing and quantum information.

## B. Brillouin cooling

Many quantum experiments can only be carried out at low temperatures (passive cooling) in order to reduce the decoherence effect introduced by thermal noise. Laser cooling is one of the most promising active cooling techniques [6] to reduce thermal noise in a specific frequency band. Recently, laser cooling induced by anti-Stokes Brillouin scattering, i.e., Brillouin cooling, has been explored in optomechanical waveguides [8,29] by utilizing forward Brillouin scattering where phonons experience lower damping than photons.

However, Brillouin cooling generated by backward Brillouin scattering where the acoustic dissipation exceeds the optical dissipation in typical Brillouin-active waveguides is still largely unexplored. In this section, we propose a cooling mechanism by using pulses rather than continuous waves. We claim that this cooling mechanism might attain higher cooling efficiency and can be used in long fibers.

Conventional laser cooling is based on increasing the effective dissipation of phonons by using a damping laser. Here we propose an alternative cooling mechanism based on coherent transfer. As shown in the previous section, the anti-Stokes process can be regarded as a photon-phonon Rabi oscillation using the linearized effective Hamiltonian. The main idea of coherent transfer-based cooling is to use a carefully designed laser pulse to convert phonons to photons through the phonon-photon Rabi oscillations. In this section, we will show how to use our formalism to investigate the Brillouin cooling in waveguides. Such Brillouin cooling approach in waveguides in the pulse regime is similar to the dynamical cooling method in cavity optomechanical systems [45]. The convenience in experiment of this dynamical Brillouin cooling approach in waveguides will prompt the elegant transient cooling technique to become an effective experimental tool in continuum optomechanical systems. Our laser pulses at the appropriate pulse length will avoid reverse conversion, thus leaving fewer phonons in the waveguide system. By using a pulsed pump, the pump depletion effect due to the Stokes process can also be avoided. The cooling process is illustrated using space-time diagram in Fig. 6.

The cooling effect can be quantified by counting the remained phonons. We introduce the spectrum remained phonon rates  $\kappa(\Delta, \eta)$ ,

$$\begin{aligned}\kappa(\Delta, \eta) &= \frac{\langle \tilde{b}^\dagger(\Delta, \eta)\tilde{b}(\Delta, \eta) \rangle}{\langle \tilde{b}^\dagger(\Delta, 0)\tilde{b}(\Delta, 0) \rangle} \\ &= |\mathbf{G}_{22}(\Delta, \eta)|^2 + \Gamma \int_0^\eta d\nu |\mathbf{G}_{22}(\Delta, \nu)|^2 \\ &= \kappa_c + \kappa_n,\end{aligned}\quad (45)$$

which is defined as the ratio of the cooled phonon occupation at  $\eta$  to the initial thermal phonon occupancy ( $n_{th}$ ). The smaller the  $\kappa(\Delta, \eta)$ , the better cooling effect is achieved.

Equation (45) consists of two terms: the first term  $\kappa_c$  describes how fast the coherent transfer/cooling is able to convert the phonons into photons (which are then removed from the system); the second term  $\kappa_n$  describes how fast the phonons are restored due to the interaction with the thermal environment, which is the thermal noise term that obstructing the cooling of the system. Figure 8 shows the two terms and the whole  $\kappa(\Delta = 0, t)$  at the perfect phase-matching point  $\Delta = 0$ . One can clearly see the Rabi oscillation behavior of the coherent part, which contributes to cooling, and the accumulating thermal noise counterbalances the cooling effect, which eliminates the cooling effect when the pulse length increases.

In conventional fiber optic systems, the dissipation rate of the optical channel is much smaller than the dissipation rate of the acoustic channel,  $\gamma \ll \Gamma$ . With this approximation,

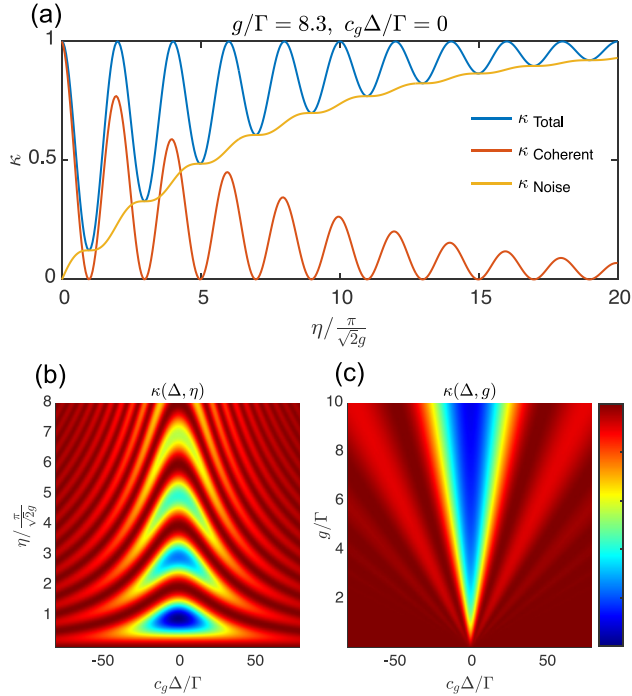


FIG. 8. The Brillouin cooling. (a) The remained phonon consists of two parts: the coherent part determined by the initial state and the noise generated part. Optimal cooling can be achieved by choosing appropriate pump length to be  $\pi/2$  Rabi period. (b) The transfer efficiency was calculated using  $g = 8.3\Gamma$  (Chalcogenide chip [35] with pump power equals 1 W). A clear oscillating behavior due to the Rabi nature can be seen. (c) The cooling effect on different parameters, when pump length equals the  $\pi/2$  Rabi pulse  $\eta = \pi/\sqrt{2}g$ . As the coupling strength increases, the effective cooling bandwidth will increase.

spectrum remained phonon rate reads

$$\kappa(\Delta, \eta) \approx 1 - \left| e^{-\frac{\Gamma_{e,as}\eta}{2}} \frac{8g_{e,as}^2 + \Gamma_{e,as}^2}{8g_{e,as}^2} \sin^2\left(\frac{g_{e,as}\eta}{\sqrt{2}}\right) \right|. \quad (46)$$

The  $g_{e,as}$  and  $\Gamma_{e,as}$  is defined in Eq. (43). The detailed derivation for the above result can be found in the Appendix C. Equation (46) shows that choosing

$$\eta = (2n + 1) \frac{\pi}{\sqrt{2}g} \quad (n \in \mathbb{Z}), \quad (47)$$

leads to the minimum  $\kappa(\Delta, \eta)$ , which is equivalent to the maximum cooling efficiency. Due to the accumulating thermal noise, minimum  $\kappa(\Delta = 0, \eta)$  can be achieved near the first Rabi  $\pi/2$  pulse at  $\eta \approx \pi/(\sqrt{2}g)$ , this is the same as the maximum coherent transfer efficiency shown in Eq. (44), which is also based on the same photon-phonon Rabi oscillation.

In Figs. 8(b) and 8(c), we present the calculated  $\kappa(\Delta, \eta)$  for different coupling strength and pulse length by assuming rectangular pump pulse. Due to the decoherence effect of thermal noise, the optimal cooling pulse is the  $\pi/2$  Rabi pulse, which refers to  $n = 1$  case in Eq. (47). From Fig. 8(c), one can clearly see that the cooling bandwidth becomes wider for stronger coupling, which indicates a wider interaction bandwidth. We claim that this has the same mathematical roots as the general power broadening effect in all atomic systems

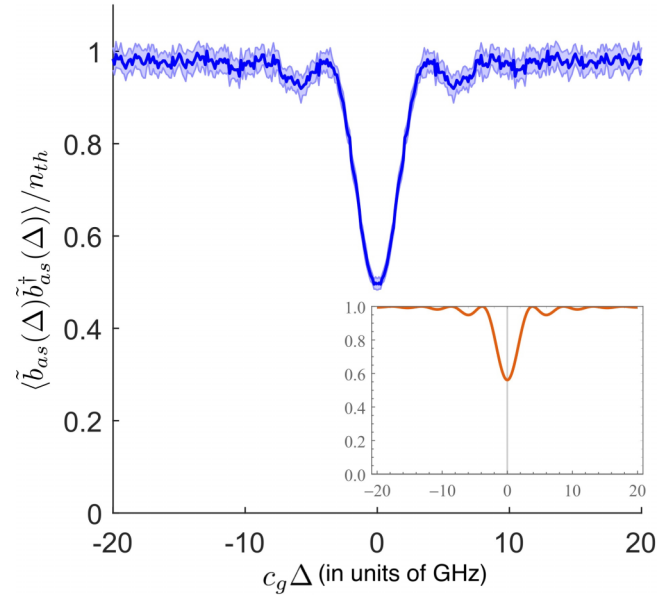


FIG. 9. The remained phonon spectrum after a  $\pi/2$  cooling pulse. This figure is obtained by the first-principle simulation using the algorithm from Ref. [46,47]. In the simulation, a chalcogenide waveguide [35] with length  $L = 1$  m is assumed. A  $\pi/2$  Rabi pulse with pump power  $I_p = 10$  W, pulse length  $t = \frac{\pi}{\sqrt{2}g}$  is used as the cooling pulse. The phonon spectrum is calculated when the pump pulse leaves the fiber at  $t = L/c_g$ . The shaded area indicates the  $3\sigma$  error, and the theoretically predicted result is shown in the lower right corner. By applying a rectangular cooling pulse, the remaining phonon spectrum is sinc like, and around 50% of the initial phonon number at the central wave vector has been removed.

[48]. The thermal noise can be represented by zero-mean space-time white noise [46] in the simulation of the coupled mode equation [47]. We simulate the pulse propagation process in a chalcogenide waveguide [35] and calculate the phonon spectrum after one cooling pulse passes. The result is shown in Fig. 9, which is consistent with our analytical expressions.

### C. Entanglement

Quantum entanglement is one of the fundamental building blocks of today's quantum technologies, especially quantum communication. The generation of entangled quantum pairs is the basis of quantum state teleportation and quantum repeaters. Classical information networks based on optical fibers are one of the most promising infrastructures for future quantum teleportation, which means that generating entangled pairs in an all-fiber system is a fruitful challenge. Apart from the application-based perspective, achieving the generation of entangled pairs is also one of the vital experiments to demonstrate the ability to do quantum experiments in optomechanical waveguides.

In this section, we show that the photon-phonon entangled pair generation can be achieved by utilizing the Stokes process, and the entangled photon-phonon pairs can be further transformed into photon-photon entangled pairs by the coherent transfer technique described in Sec. III A, as shown

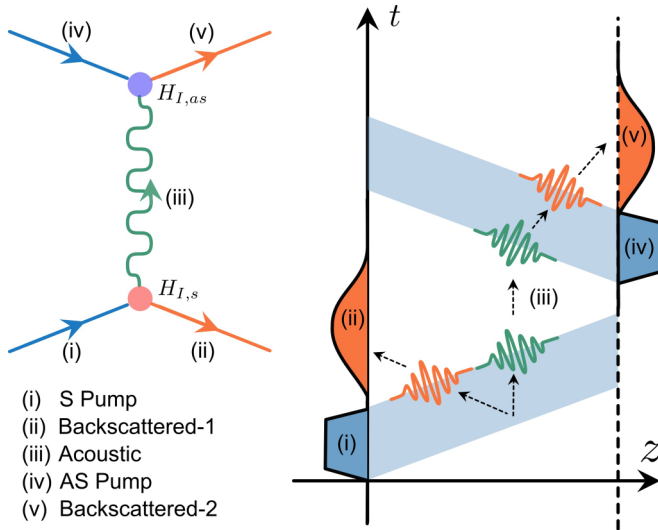


FIG. 10. Illustration of the entangled pair generation process. First, a blue-detuned pump pulse (S pump) should be applied to generate the entangled phonon-photon pairs via the Stokes interaction  $H_{I,s}$ . Then, a red-detuned pump pulse (AS pump) should be applied to stimulate the coherent transfer process via anti-Stokes interaction  $H_{I,as}$  described in the previous sections to readout the phonon into a photon. By combining these two processes, the measurable entangled photons pairs (Backscattered-1 and Backscattered-2) could be generated.

in terms of the space-time diagram in Fig. 10. Choosing the Stokes process to generate photon-phonon pairs is motivated by the down-conversion nature of the Stokes process. In the Stokes process, a higher energy phonon and a lower frequency photon must be satisfied, which leads to the phase-matching condition. As a direct result of this phase-matching condition, there is some shared information between the produced phonon and photon, which leads to quantum entanglement.

We introduce the quadrature operators for the acoustic field and the optical field

$$\begin{aligned} X_a &= \frac{a + a^\dagger}{\sqrt{2}}, & Y_a &= i \frac{a^\dagger - a}{\sqrt{2}}, \\ X_b &= \frac{b + b^\dagger}{\sqrt{2}}, & Y_b &= i \frac{b^\dagger - b}{\sqrt{2}}. \end{aligned} \quad (48)$$

To prove the existence of quantum entanglement, we use Duan's two-mode entanglement criterion [49]. The main idea of the Duan's criterion is to choose two EPR variables and calculate the variance sum. It can be shown that once the correlation variance is less than a specific quantum limit, the density matrix of the two quantum modes cannot be separated by any means, thus leading to quantum entanglement.

The two mode EPR variables we choose are

$$u = \frac{1}{\alpha} X_a + \alpha Y_b, \quad v = \frac{1}{\alpha} Y_a + \alpha X_b, \quad (49)$$

with  $\alpha = 2^{-1/4}$ . This particular  $\alpha$  value is obtained by trying to minimize the EPR variance. The Duan's entanglement cri-

terion [49] for it is

$$\sigma_{\text{EPR}}^2 = \frac{\sigma^2 u + \sigma^2 v}{\alpha^2 + \alpha^{-2}} < 1. \quad (50)$$

After some calculations, the expression of  $\sigma_{\text{EPR}}^2$  reads

$$\begin{aligned} \sigma_{\text{EPR}}^2 &= \frac{1}{3} |\sqrt{2} \mathbf{G}_{11} + i \mathbf{G}_{21}|^2 + \frac{2n_0 + 1}{3} |\sqrt{2} \mathbf{G}_{12} + i \mathbf{G}_{22}|^2 \\ &\quad + \frac{2n_{th} + 1}{3} \Gamma \int_0^\eta d\nu |\sqrt{2} \mathbf{G}_{12} + i \mathbf{G}_{22}|^2 \\ &\approx \left(1 + \frac{2n_0}{3}\right) |G(\eta)|^2 + \frac{2n_{th} + 1}{3} \Gamma \int_0^\eta d\nu |G(\nu)|^2, \end{aligned} \quad (51)$$

where

$$G(\eta) = e^{-\frac{1}{4} \Gamma_{e,s} \eta} \left[ e^{-\frac{g_{e,s} \eta}{\sqrt{2}}} - \frac{\Gamma_{e,s}}{2\sqrt{2} g_{e,s}} \sinh\left(\frac{g_{e,s} \eta}{\sqrt{2}}\right) \right]. \quad (52)$$

The detailed calculation can be found in Appendix D. The  $n_0$  is the phonon number expectation at the initial state  $\eta = 0$ , and the  $n_{th}$  is the thermal phonon expectation number determined by the temperature of the environment. When the system is cooled by the cooling technique we proposed in the previous sections,  $n_0 < n_{th}$  can be achieved. The off-resonance effective coupling and the effective dissipation for the Stokes process shown here are slightly different from what we defined in the anti-Stokes process in Eq. (43),

$$\begin{aligned} g_{e,s} &= \sqrt{g^2 + (\Gamma + ic_g \Delta)^2 / 8}, \\ \Gamma_{e,s} &= \Gamma + ic_g \Delta. \end{aligned} \quad (53)$$

The  $G(\eta)$  consists of two competing terms. The first term shows an exponential depressing of the EPR variance with rate  $g_{e,s}$  while the sinh-like second term will refer to the decoherence effect that will destroy such entanglement. Therefore the photon-phonon entangle can be achieved by choosing adequate pump length in the Stokes process.

We present the numerical result for the photon-phonon entangled EPR variance in Fig. 11. The dashed lines in Figs. 11(b) and 11(c) refer to the quantum nonseparation limit  $\sigma_{\text{EPR}}^2 = 1$ . The generation of photon-phonon entangled pairs is based on a down-conversion-like Stokes process rather than a beam-splitter-like anti-Stokes process. Therefore, unlike the coherent transport and cooling discussed in the previous sections, there is no Rabi oscillation behavior. As shown in the Fig. 11(a), the longer pulse will induce a stronger entangled effect while decreasing the entangled bandwidth, and stronger coupling can still broaden the entangled bandwidth. In practice, the optimal entangled pulse length should be specified by taking the measurement bandwidth of the experiment setup into consideration: The photon-phonon entangled pair cannot be measured directly, the coherent transfer process is needed to transfer the entangled phonon into a photon, in which the measurement bandwidth can be controlled by manipulating the pump waveform as discussed in previous sections. We show in Fig. 11 the results of photon-phonon entangled pair generation obtained by direct computation with the noisy Brillouin simulation algorithm [46]. The simulation combines photon-phonon entangled pair generation with the

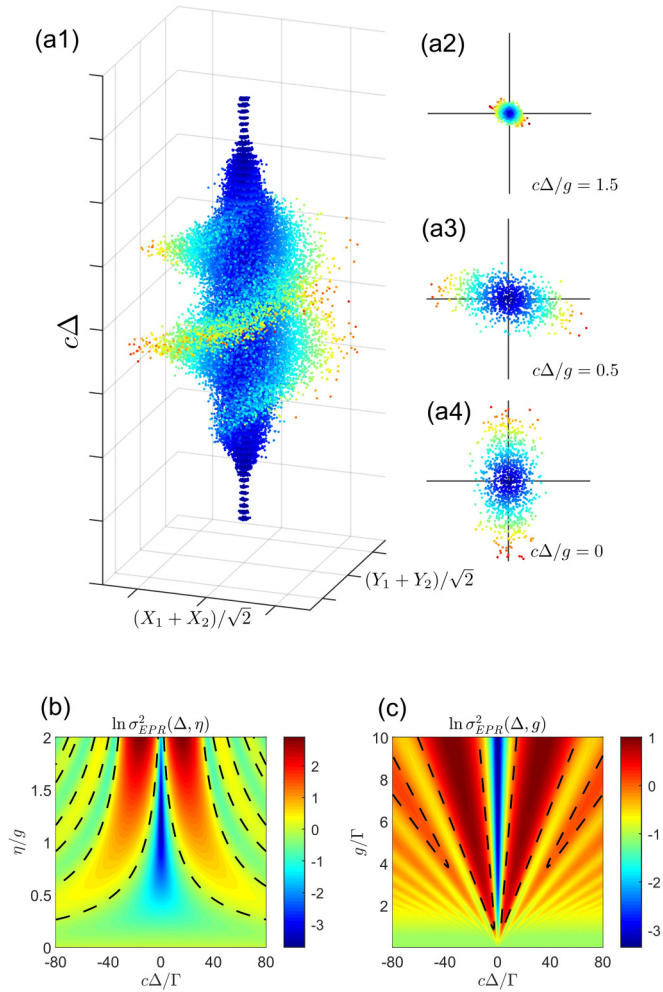


FIG. 11. The Brillouin entanglement. (a1) The quadrature distribution in different  $\Delta$  is shown using algorithm from Ref. [46,47]. The simulation parameter is the same as Fig. 9.  $X_1, X_2, Y_1, Y_2$  are the quadrature components of the two backscattered pulses. Nonuniform distribution of quadratures can be seen when  $|\Delta| < \Gamma$ , which implies shared information between two scattered photons. When  $|\Delta|$  is large, the Brillouin interaction strength is limited by the phase-matching condition, so the two-mode correlation between quadratures gradually disappears. The discretization along the frequency axis ( $c_g\Delta$ ) is the result of the Fourier transform of the finite numerical simulation time. (a2)–(a4) is the transection of (a1) at the three points of wavevector  $|\Delta|$  from larger to smaller. [(b),(c)] The EPR variance  $\sigma_{EPR}^2$ . As the coupling increases, the effective entangled spectrum bandwidth will increase. (b) is calculated using  $g = 8.3\Gamma$  (Chalcogenide chip [35] with pump power equals 1W).

coherent transfer, which is directly computed for photon-phonon entangled pairs.

Actually, the thermal noise of the acoustic field can cause a destructive effect on the optomechanical entanglement in the long time evolution of the system, as shown in Fig. 11(b). However, different from the case discussed in Ref. [50,51] in cavity optomechanical systems, which considers the weak coupling regime, we generate the optomechanical entanglement in the strong coupling regime similar to the optical entanglement in optomechanical systems

discussed in Ref. [52,53]. This strong Brillouin optomechanical interaction in the pulsed regime induces an extra suppression to the destructive effect of thermal noise, which enables the robust optomechanical entanglement at a high environmental temperature in continuum optomechanical systems. In addition to that, Brillouin optomechanics operates in the several GHz frequency range, which has the advantage of a lower thermal phonon number from the start.

#### IV. CONCLUSIONS AND PERSPECTIVES

In this paper, we proposed a formulation to treat traveling phonons and traveling photons in a optomechanical waveguide system as an array of multiple optomechanical cavities. The possibility of realizing coherent control using this formulation has been shown: Both the effective coupling strength and the interaction time can be controlled easily by manipulating the shape of the pump pulse. By applying the formulation, we show that it is possible to achieve active Brillouin cooling through the backward Brillouin scattering process and quantum entangled pair generation in waveguide systems. Experiments based on this formalism are shown to be achievable using current technology and fabrication of optical fibers and integrated waveguides.

Our paper mainly focuses on the backward scattering optomechanical interaction and most of the calculations are done using the assumption that the pump pulse is almost nondepleted. The undepleted assumption leads to a linearized Hamiltonian directly, which is similar to down-conversion for the Stokes process and similar to a beam-splitter for the anti-Stokes process. The available quantum operation time approximately equals the ratio between the coupling strength and the dissipation rate,  $N_{op} = g/\Gamma$ . There are two routes, including the dissipation reduction and coupling enhancement, towards a broader range of quantum applications within optomechanical waveguides. In order to reduce the dissipation rate, efforts have to be paid in designing waveguides that can localize and trap acoustic phonons with high efficiency. In order to increase the coupling strength, one method is to increase the material-dependent coupling strength  $g_0$  by optimizing the waveguide structure or using more promising materials [54]. Another method to increase the coupling strength is to use higher pump powers. In this case, the pump light may be significantly depleted, so shorter light pulses are needed to meet the requirements of coherent control. Therefore, the undepleted regime within the short pulses regime (below 100 ps) need to be considered in future works.

Because all Brillouin backscattering processes under undepleted conditions can be solved exactly based on the method of this paper, future efforts should be spent on detailed modeling of the Brillouin memory process, where information is coherently stored in acoustic waves [20,21]. In particular, the method can be the base for a model including quantum noise and a study on how coherent information is destroyed by different noise contributions.

The data and source codes for all the figures in this paper are available as Supplemental Material [55].

### ACKNOWLEDGMENTS

Authors acknowledge funding from the Max Planck Gesellschaft through an independent Max Planck Research Group, CW acknowledges funding from the Villum Fonden related to Grant No. 16498.

### APPENDIX A: DETAILED DETIVATION OF THE COORDINATES TRANSFORMATION

In this Appendix, we detailed coordinate transformation for linearized Stokes process, from Eq. (10) to Eq. (13). The derivation for the anti-Stokes process can be obtained in the same way.

The linearized coupled mode equation for Stokes process in Eq. (10) reads

$$\begin{aligned} \partial_t a_s - c_g \partial_z a_s &= -igb_s^\dagger - \gamma/2 a_s, \\ \partial_t b_s &= -iga_s^\dagger - \Gamma/2 b_s + \sqrt{\Gamma} \xi. \end{aligned} \quad (\text{A1})$$

Since the pump pulse propagates along the fiber in a constant velocity  $c_g$  without changing the shape, the pump-related coupling term  $g(z, t)$  satisfies the comoving condition

$$g(z, t) = g(0, t - z/c_g). \quad (\text{A2})$$

To fully take advantage of this comoving relationship, we introduced the coordinate transformation as in Eq. (11),

$$\eta = t - z/c_g, \quad \tau = t. \quad (\text{A3})$$

In this transformation, the derivative operators are related by

$$\begin{aligned} \partial_t &= \frac{\partial \eta}{\partial t} \partial_\eta + \frac{\partial \tau}{\partial t} \partial_\tau, \\ \partial_z &= \frac{\partial \eta}{\partial z} \partial_\eta + \frac{\partial \tau}{\partial z} \partial_\tau, \end{aligned} \quad (\text{A4})$$

which is

$$\begin{pmatrix} \partial_z \\ \partial_t \end{pmatrix} = \begin{pmatrix} -1/c_g & 0 \\ 1 & 1 \end{pmatrix} \begin{pmatrix} \partial_\eta \\ \partial_\tau \end{pmatrix}. \quad (\text{A5})$$

By substituting  $\partial_z$  and  $\partial_t$  in Eq. (10), we get Eq. (13),

$$\begin{aligned} (\partial_\tau + 2\partial_\eta) a_s &= -igb_s^\dagger - \gamma/2 a_s, \\ (\partial_\tau + \partial_\eta) b_s^\dagger &= iga_s - \Gamma/2 b_s^\dagger + \sqrt{\Gamma} \xi^\dagger. \end{aligned} \quad (\text{A6})$$

### APPENDIX B: DETAILED DERIVATION OF THE UNDEPLETED CONDITIONS

The backscattered Stokes power is the integral of photon densities

$$I_S = \int_{-\infty}^{+\infty} d\Delta \frac{\hbar \omega c_g}{2\pi} \langle \tilde{a}_s^\dagger(\Delta) \tilde{a}_s(\Delta) \rangle. \quad (\text{B1})$$

Using the technique we developed, we have

$$\begin{aligned} \langle \tilde{a}_s^\dagger(\Delta, \eta) \tilde{a}_s(\Delta, \eta) \rangle &= |\mathbf{G}_{12}(\Delta, \eta)|^2 \langle \tilde{b}_s^\dagger(\Delta, 0) \tilde{b}_s(\Delta, 0) \rangle \\ &+ n_{th} \Gamma \int_0^t d\nu |\mathbf{G}_{12}(\Delta, \nu)|^2. \end{aligned} \quad (\text{B2})$$

For the system driven by short pulses  $\eta \sim 1/g \ll 1/\Gamma$  in strong coupling regime, the second term, which is the noise

contribution can be omitted. The average thermal phonon number at  $t = 0$  reads

$$\langle \tilde{b}_s^\dagger(\Delta, 0) \tilde{b}_s(\Delta, 0) \rangle = \frac{1}{\exp \frac{\hbar \Omega}{k_B T_E} - 1} \approx \frac{k_B T_E}{\hbar \Omega}. \quad (\text{B3})$$

Therefore the spectrum density of Stokes photon reads

$$\langle \tilde{a}_s^\dagger(\Delta, \eta) \tilde{a}_s(\Delta, \eta) \rangle \approx \frac{k_B T_E}{\hbar \Omega} |\mathbf{G}_{12}(\Delta, \eta)|^2. \quad (\text{B4})$$

For  $g \ll \Gamma$ , the following approximation holds:

$$\mathbf{G}_{12}(\Delta, \eta) \approx \frac{2g \sinh \frac{1}{4} \sqrt{8g^2 - c^2 \Delta^2} t}{\sqrt{8g^2 - c^2 \Delta^2}}. \quad (\text{B5})$$

The peak of  $\mathbf{G}_{12}(\Delta, \eta)$  is

$$\mathbf{G}_{12}(\Delta = 0, \eta) = \frac{i \sinh \frac{g\eta}{\sqrt{2}}}{\sqrt{2}} \approx \frac{ie^{g\eta/\sqrt{2}}}{2\sqrt{2}}. \quad (\text{B6})$$

The width of the central peak can be approximated by solving  $8g^2 - c^2 \Delta^2 = 0$ ,

$$\text{Wd.} \approx 2 \times \frac{2\sqrt{2}g}{c}. \quad (\text{B7})$$

Finally we have

$$\begin{aligned} I_S &\approx \int_{-\infty}^{+\infty} d\Delta \frac{\hbar \omega c_g}{2\pi} \frac{k_B T_E}{\hbar \Omega} |\mathbf{G}_{21}(\Delta, \eta)|^2 \\ &\approx \frac{\hbar \omega c_g}{4\pi} \frac{k_B T_E}{\hbar \Omega} (\text{Wd.} \times |\mathbf{G}_{12}(\Delta=0, \eta)|^2) = \frac{e^{\sqrt{2}g\eta} g k_B T_E \omega}{2\sqrt{2}\pi \Omega}. \end{aligned} \quad (\text{B8})$$

The undepleted condition is satisfied if and only if the backscattered Stokes power is much smaller than the pump power,  $I_S \ll I_p$ . Since the effective coupling  $g$  is related to the pump power  $I_p$  by

$$g = \sqrt{\frac{G I_p \Gamma c_g}{4}}, \quad (\text{B9})$$

where the  $G$  is the Brillouin gain with unit  $[\text{m}^{-1}\text{W}^{-1}]$ , the above undepleted condition can be simplified to

$$g\eta \ll \frac{1}{2\sqrt{2}} \ln \frac{32\pi^2 I_p \Omega^2}{G \Gamma c_g k_B^2 T_E^2 \omega^2}. \quad (\text{B10})$$

### APPENDIX C: DETAILED DERIVATION FOR BRILLOUIN COOLING

In this section, we present the detailed derivation process for Brillouin cooling. Because the phonons in the anti-Stokes process and Stokes process are separated by their opposite travel direction, we can only consider the anti-Stokes process, which describes the photon-phonon transfer.

The phenomenologically introduced effective Hamiltonian for anti-Stokes process reads [Eq.(16)]

$$\begin{aligned} \frac{\partial}{\partial \eta} \begin{pmatrix} \tilde{a}_{as}(\Delta, \eta) \\ \tilde{b}_{as}(\Delta, \eta) \end{pmatrix} &= \begin{pmatrix} -ic_g \Delta/2 - \gamma/4 & -ig/2 \\ -ig & -ic_g \Delta - \Gamma/2 \end{pmatrix} \\ &\times \begin{pmatrix} \tilde{a}_{as}(\Delta, \eta) \\ \tilde{b}_{as}(\Delta, \eta) \end{pmatrix} + \begin{pmatrix} 0 \\ \sqrt{\Gamma} \xi \end{pmatrix}. \end{aligned} \quad (\text{C1})$$

The  $c_g$  is the group velocity of the optical field near the phase matching point. The  $g$  is the effective coupling strength enhanced by the pump power, and  $n_{th}$  is the averaged thermal phonon number. The relation between the effective coupling and the well-known Brillouin coupling strength  $G$  is [Eq. (31)]

$$g = \sqrt{\frac{G\Gamma\Gamma c_g}{4}}. \quad (C2)$$

This can be obtained by calculating the steady-state behavior of the coupled mode equation, as shown in the main context of this paper. The  $\tilde{\xi}$  describes the thermal noise, the thermal behavior of phonon determines both the initial state and the noise term, which could be described by a Wigner process

$$\begin{aligned} \langle \tilde{b}_{as}^\dagger(\Delta_1, \eta_1) \tilde{b}_{as}(\Delta_2, \eta_2) \rangle &= n_{th} \delta(\Delta_1 - \Delta_2) \delta(\eta_1 - \eta_2), \\ \langle \tilde{\xi}^\dagger(\Delta_1, \eta_1) \tilde{\xi}(\Delta_2, \eta_2) \rangle &= n_{th} \delta(\Delta_1 - \Delta_2) \delta(\eta_1 - \eta_2). \end{aligned} \quad (C3)$$

The equation is a Langevin equation. Therefore we can solve the equation using the conventional method for Langevin equations, which is the undetermined coefficient method. Considering the rectangular pump wave, we introduce the  $\mathbf{P}$  matrix as

$$\mathbf{P} = \begin{pmatrix} -ic_g\Delta/2 - \gamma/4 & -ig/2 \\ -ig & -ic_g\Delta - \Gamma/2 \end{pmatrix}. \quad (C4)$$

For a Langevin equation in the form

$$\frac{d}{d\eta} \vec{\mathbf{M}} = \mathbf{P} \vec{\mathbf{M}} + \vec{\mathbf{R}}. \quad (C5)$$

The solution reads

$$\vec{\mathbf{M}}(\eta) = \exp(\mathbf{P}\eta) \vec{\mathbf{M}}(0) + \int_0^\eta \exp[\mathbf{P}(\eta - \nu)] \vec{\mathbf{R}}(\nu) d\nu. \quad (C6)$$

Therefore we need to calculate the matrix exponential of the  $\mathbf{P}$  matrix. The matrix exponential can be calculated by using the formula

$$e^{\mathbf{S}\mathbf{D}\mathbf{S}^{-1}} = \mathbf{S}e^{\mathbf{D}}\mathbf{S}^{-1}. \quad (C7)$$

Where the Jordan decomposition is used

$$\mathbf{P} = \mathbf{S}\mathbf{D}\mathbf{S}^{-1}. \quad (C8)$$

The  $\mathbf{S}$  is the similar matrix, and  $\mathbf{D}$  is the Jordan matrix. In our case,  $\mathbf{D}$  is diagonalized. By introducing the small optical dissipation approximation

$$(\Gamma \pm \gamma) \approx \Gamma. \quad (C9)$$

Under those approximations the matrix exponential can be obtained,

$$\mathbf{G} = \exp(\mathbf{P}\eta). \quad (C10)$$

The matrix elements read

$$\begin{aligned} \mathbf{G}_{11} &= e^{-\frac{1}{4}\Gamma_{e,as}^*\eta - ic_g\Delta\eta} \left[ \cos\left(\frac{g_{e,as}\eta}{\sqrt{2}}\right) + \frac{\Gamma_{e,as}}{2\sqrt{2}g_{e,as}} \sin\left(\frac{g_{e,as}\eta}{\sqrt{2}}\right) \right], \\ \mathbf{G}_{12} &= -ie^{-\frac{1}{4}\Gamma_{e,as}^*\eta - ic_g\Delta\eta} \frac{g}{\sqrt{2}g_{e,as}} \sin\left(\frac{g_{e,as}\eta}{\sqrt{2}}\right), \\ \mathbf{G}_{21} &= -ie^{-\frac{1}{4}\Gamma_{e,as}^*\eta - ic_g\Delta\eta} \frac{g}{\sqrt{2}g_{e,as}} \sin\left(\frac{g_{e,as}\eta}{\sqrt{2}}\right), \\ \mathbf{G}_{22} &= e^{-\frac{1}{4}\Gamma_{e,as}^*\eta - ic_g\Delta\eta} \left[ \cos\left(\frac{g_{e,as}\eta}{\sqrt{2}}\right) - \frac{\Gamma_{e,as}}{2\sqrt{2}g_{e,as}} \sin\left(\frac{g_{e,as}\eta}{\sqrt{2}}\right) \right], \end{aligned} \quad (C11)$$

where

$$\begin{aligned} g_{e,as} &= \sqrt{g^2 - (\Gamma + ic_g\Delta)^2/8}, \\ \Gamma_{e,as} &= \Gamma + ic_g\Delta. \end{aligned} \quad (C12)$$

The remained phonon spectrum density can be explained as

$$\begin{aligned} \kappa(\Delta, \eta) &= \frac{\langle \tilde{b}_{as}^\dagger(\Delta, \eta) \tilde{b}_{as}(\Delta, \eta) \rangle}{\langle \tilde{b}_{as}^\dagger(\Delta, 0) \tilde{b}_{as}(\Delta, 0) \rangle} \\ &= |\mathbf{G}_{22}(\Delta, \eta)|^2 + \Gamma \int_0^\eta |\mathbf{G}_{22}(\Delta, \nu)| d\nu. \end{aligned} \quad (C13)$$

For the resonance case, when  $\Delta = 0$ , we have

$$\kappa(\Delta = 0, \eta) = 1 - e^{-\frac{\Gamma_{e,as}\eta}{2}} \frac{8g_{e,as}^2 + \Gamma^2}{8g_{e,as}^2} \sin^2\left(\frac{g_{e,as}\eta}{\sqrt{2}}\right). \quad (C14)$$

As an approximation when  $g \gg \Gamma$ ,  $g \gg |c\Delta|$ , this result can be extended to the general case by taking the norm and replacing  $\Gamma$  with  $\Gamma_{e,as}$ ,

$$\kappa(\Delta, \eta) = 1 - \left| e^{-\frac{\Gamma_{e,as}\eta}{2}} \frac{8g_{e,as}^2 + \Gamma_{e,as}^2}{8g_{e,as}^2} \sin^2\left(\frac{g_{e,as}\eta}{\sqrt{2}}\right) \right|. \quad (C15)$$

#### APPENDIX D: DETAILED DERIVATION FOR BRILLOUIN ENTANGLEMENT

In this Appendix, we present the derivation process of the Brillouin interaction based optomechanics entanglement. The entangled pair generation can be achieved by down-conversion in quantum optics. In the optomechanics waveguide systems, the Hamiltonian for Stokes process also has a down-conversion like form, the only difference is the states it acts on which are one photon and one phonon, therefore the entangled pair it generated is a photon-phonon entangled pair.

The phenomenologically introduced effective Hamiltonian for anti-Stokes process reads [Eq.(15)]

$$\begin{aligned} \frac{\partial}{\partial \eta} \begin{pmatrix} \tilde{a}_s(\Delta, \eta) \\ \tilde{b}_s^\dagger(\Delta, \eta) \end{pmatrix} &= \begin{pmatrix} -ic_g\Delta/2 - \gamma/4 & -ig/2 \\ ig & -ic_g\Delta - \Gamma/2 \end{pmatrix} \\ &\times \begin{pmatrix} \tilde{a}_s(\Delta, \eta) \\ \tilde{b}_s^\dagger(\Delta, \eta) \end{pmatrix} + \begin{pmatrix} 0 \\ \sqrt{\Gamma}\tilde{\xi}^\dagger \end{pmatrix}. \end{aligned} \quad (D1)$$

The thermal noise is introduced as the following:

$$\begin{aligned} \langle \tilde{b}_s^\dagger(\Delta_1, \eta_1) \tilde{b}_s(\Delta_2, \eta_2) \rangle &= n_0 \delta(\Delta_1 - \Delta_2) \delta(\eta_1 - \eta_2), \\ \langle \tilde{\xi}^\dagger(\Delta_1, \eta_1) \tilde{\xi}(\Delta_2, \eta_2) \rangle &= n_{th} \delta(\Delta_1 - \Delta_2) \delta(\eta_1 - \eta_2). \end{aligned} \quad (\text{D2})$$

The  $n_0$  is the phonon number expectation at the initial state  $\eta = 0$ , and the  $n_{th}$  is the thermal phonon expectation number determined by the temperature of the environment. When the system is cooled by the cooling technique we proposed in the previous sections,  $n_0 < n_{th}$  can be achieved.

The quantum noise is introduced as the following:

$$\begin{aligned} [\tilde{b}_s(\Delta_1, \eta_1), \tilde{b}_s^\dagger(\Delta_2, \eta_2)] &= \delta(\Delta_1 - \Delta_2) \delta(\eta_1 - \eta_2), \\ [\tilde{\xi}(\Delta_1, \eta_1), \tilde{\xi}^\dagger(\Delta_2, \eta_2)] &= \delta(\Delta_1 - \Delta_2) \delta(\eta_1 - \eta_2). \end{aligned} \quad (\text{D3})$$

The  $n_0$  refers to the average thermal phonon at phase-matching point at  $t = 0$ . It is possible for  $n_0 < n_{th}$  when the system is precooled by the laser cooling process, such as the coherent transfer-based Brillouin cooling we present in this paper. The exact expression for the matrix reads

$$\begin{aligned} \mathbf{G}_{11} &= e^{-\frac{1}{4}\Gamma_{e,s}^* \eta - ic_g \Delta \eta} \left[ \cosh\left(\frac{g_{e,s} \eta}{\sqrt{2}}\right) + \frac{\Gamma_{e,s}}{2\sqrt{2}g_{e,s}} \sinh\left(\frac{g_{e,s} \eta}{\sqrt{2}}\right) \right], \\ \mathbf{G}_{12} &= -ie^{-\frac{1}{4}\Gamma_{e,s}^* \eta - ic_g \Delta \eta} \frac{g}{\sqrt{2}g_{e,s}} \sinh\left(\frac{g_{e,s} \eta}{\sqrt{2}}\right), \end{aligned}$$

$$\begin{aligned} \mathbf{G}_{21} &= ie^{-\frac{1}{4}\Gamma_{e,s}^* \eta - ic_g \Delta \eta} \frac{\sqrt{2}g}{g_{e,s}} \sinh\left(\frac{g_{e,s} \eta}{\sqrt{2}}\right), \\ \mathbf{G}_{22} &= e^{-\frac{1}{4}\Gamma_{e,s}^* \eta - ic_g \Delta \eta} \left[ \cosh\left(\frac{g_{e,s} \eta}{\sqrt{2}}\right) - \frac{\Gamma_{e,s}}{2\sqrt{2}g_{e,s}} \sinh\left(\frac{g_{e,s} \eta}{\sqrt{2}}\right) \right], \end{aligned} \quad (\text{D4})$$

where

$$\begin{aligned} g_{e,s} &= \sqrt{g^2 + (\Gamma + ic_g \Delta)^2 / 8}, \\ \Gamma_{e,s} &= \Gamma + ic_g \Delta. \end{aligned} \quad (\text{D5})$$

The two mode EPR variables we choose are

$$u = \frac{1}{\alpha} X_a + \alpha Y_b, \quad v = \frac{1}{\alpha} Y_a + \alpha X_b, \quad (\text{D6})$$

with  $\alpha = 2^{-1/4}$ . The  $u, v$  can be written as

$$\begin{aligned} u &= 2^{-1/2} [(2^{1/4} \tilde{a}_s + 2^{-1/4} i \tilde{b}_s^\dagger) + \text{H.c.}], \\ v &= 2^{-1/2} [-i(2^{1/4} \tilde{a}_s + 2^{-1/4} i \tilde{b}_s^\dagger) + \text{H.c.}]. \end{aligned} \quad (\text{D7})$$

We have

$$\begin{aligned} 2^{1/4} \tilde{a}_s(\Delta, \eta) + 2^{-1/4} i \tilde{b}_s(\Delta, \eta) &= 2^{-1/4} (\sqrt{2} \mathbf{G}_{11} + i \mathbf{G}_{21}) \tilde{a}_s(\Delta, 0) + 2^{-1/4} (\sqrt{2} \mathbf{G}_{12} + i \mathbf{G}_{22}) \tilde{b}_s^\dagger(\Delta, 0) \\ &\quad + 2^{-1/4} \sqrt{\Gamma} \int_0^\eta dv (\sqrt{2} \mathbf{G}_{12} + i \mathbf{G}_{22}) \tilde{\xi}_b^\dagger(\Delta, v). \end{aligned} \quad (\text{D8})$$

The EPR variance is defined as

$$\sigma_{\text{EPR}}^2 = \frac{\sigma^2 u + \sigma^2 v}{\alpha^2 + \alpha^{-2}}. \quad (\text{D9})$$

For the entangled state, the Duan's criterion yields

$$\sigma_{\text{EPR}}^2 < 1. \quad (\text{D10})$$

Using the commutation relation, we obtained the  $\Delta_{\text{EPR}}$  as

$$\sigma_{\text{EPR}}^2 = \frac{1}{3} |\sqrt{2} \mathbf{G}_{11} + i \mathbf{G}_{21}|^2 + \frac{1}{3} (2n_0 + 1) |\sqrt{2} \mathbf{G}_{12} + i \mathbf{G}_{22}|^2 + \frac{1}{3} \Gamma (2n_{th} + 1) \int_0^\eta dv |\sqrt{2} \mathbf{G}_{12} + i \mathbf{G}_{22}|^2. \quad (\text{D11})$$

We have

$$\begin{aligned} \sqrt{2} \mathbf{G}_{11} + i \mathbf{G}_{21} &= \sqrt{2} e^{-\frac{1}{4}\Gamma_{e,s}^* \eta - ic_g \Delta \eta} \left[ \cosh\left(\frac{g_{e,s} \eta}{\sqrt{2}}\right) - \frac{g}{g_{e,s}} \sinh\left(\frac{g_{e,s} \eta}{\sqrt{2}}\right) + \frac{\Gamma_{e,s}}{2\sqrt{2}g_{e,s}} \sinh\left(\frac{g_{e,s} \eta}{\sqrt{2}}\right) \right], \\ \sqrt{2} \mathbf{G}_{12} + i \mathbf{G}_{22} &= ie^{-\frac{1}{4}\Gamma_{e,s}^* \eta - ic_g \Delta \eta} \left[ \cosh\left(\frac{g_{e,s} \eta}{\sqrt{2}}\right) - \frac{g}{g_{e,s}} \sinh\left(\frac{g_{e,s} \eta}{\sqrt{2}}\right) - \frac{\Gamma_{e,s}}{2\sqrt{2}g_{e,s}} \sinh\left(\frac{g_{e,s} \eta}{\sqrt{2}}\right) \right]. \end{aligned} \quad (\text{D12})$$

When  $g \gg \Gamma$ , we have

$$\begin{aligned} \frac{\sqrt{2}}{2} |\sqrt{2} \mathbf{G}_{11} + i \mathbf{G}_{21}| &\approx |\sqrt{2} \mathbf{G}_{12} + i \mathbf{G}_{22}| \\ &\approx e^{-\frac{1}{4}\Gamma_{e,s}^* \eta} \left| e^{-\frac{g_{e,s} \eta}{\sqrt{2}}} - \frac{\Gamma_{e,s}}{2\sqrt{2}g_{e,s}} \sinh\left(\frac{g_{e,s} \eta}{\sqrt{2}}\right) \right|. \end{aligned} \quad (\text{D13})$$

Therefore the EPR variance reads

$$\begin{aligned}\sigma_{\text{EPR}}^2 &= \frac{1}{3} \left| \sqrt{2}\mathbf{G}_{11} + i\mathbf{G}_{21} \right|^2 + \frac{1}{3} (2n_0 + 1) \left| \sqrt{2}\mathbf{G}_{12} + i\mathbf{G}_{22} \right|^2 + \frac{1}{3} \Gamma (2n_{th} + 1) \int_0^\eta dv \left| \sqrt{2}\mathbf{G}_{12} + i\mathbf{G}_{22} \right|^2 \\ &\approx \left( \frac{2}{3} n_0 + 1 \right) |G(t)|^2 + \frac{1}{3} (2n_{th} + 1) \Gamma \int_0^\eta dv |G(v)|^2,\end{aligned}\quad (\text{D14})$$

where

$$G(\eta) = e^{-\Gamma_{e,s}^* \eta/4} \left[ e^{-\frac{g_{e,s} \eta}{\sqrt{2}}} - \frac{\Gamma_{e,s}}{2\sqrt{2}g_{e,s}} \sinh\left(\frac{g_{e,s} \eta}{\sqrt{2}}\right) \right]. \quad (\text{D15})$$

- 
- [1] N. Gisin and R. Thew, Quantum communication, *Nat. Photonics* **1**, 165 (2007).
- [2] H.-S. Zhong, H. Wang, Y.-H. Deng, M.-C. Chen, L.-C. Peng, Y.-H. Luo, J. Qin, D. Wu, X. Ding, Y. Hu *et al.*, Quantum computational advantage using photons, *Science* **370**, 1460 (2020).
- [3] N. Maluf, *An Introduction to Microelectromechanical Systems Engineering*, Artech House MEMS library (Artech House, London, 2000).
- [4] A. A. Clerk, M. H. Devoret, S. M. Girvin, F. Marquardt, and R. J. Schoelkopf, Introduction to quantum noise, measurement, and amplification, *Rev. Mod. Phys.* **82**, 1155 (2010).
- [5] M. Poot and H. S. van der Zant, Mechanical systems in the quantum regime, *Phys. Rep.* **511**, 273 (2012).
- [6] M. Aspelmeyer, T. J. Kippenberg, and F. Marquardt, Cavity optomechanics, *Rev. Mod. Phys.* **86**, 1391 (2014).
- [7] T. A. Palomaki, J. D. Teufel, R. W. Simmonds, and K. W. Lehnert, Entangling mechanical motion with microwave fields, *Science* **342**, 710 (2013).
- [8] N. T. Otterstrom, R. O. Behunin, E. A. Kittlaus, and P. T. Rakich, Optomechanical Cooling in a Continuous System, *Phys. Rev. X* **8**, 041034 (2018).
- [9] S. J. M. Habraken, K. Stannigel, M. D. Lukin, P. Zoller, and P. Rabl, Continuous mode cooling and phonon routers for phononic quantum networks, *New J. Phys.* **14**, 115004 (2012).
- [10] H. Zoubi and K. Hammerer, Quantum Nonlinear Optics in Optomechanical Nanoscale Waveguides, *Phys. Rev. Lett.* **119**, 123602 (2017).
- [11] M. Li, W. H. P. Pernice, C. Xiong, T. Baehr-Jones, M. Hochberg, and H. X. Tang, Harnessing optical forces in integrated photonic circuits, *Nature (London)* **456**, 480 (2008).
- [12] M. S. Kang, A. Nazarkin, A. Brenn, and P. S. J. Russell, Tightly trapped acoustic phonons in photonic crystal fibres as highly nonlinear artificial Raman oscillators, *Nat. Phys.* **5**, 276 (2009).
- [13] E. A. Kittlaus, N. T. Otterstrom, P. Kharel, S. Gertler, and P. T. Rakich, Non-reciprocal interband Brillouin modulation, *Nat. Photonics* **12**, 613 (2018).
- [14] A. Kobyakov, M. Sauer, and D. Chowdhury, Stimulated Brillouin scattering in optical fibers, *Adv. Opt. Photon.* **2**, 1 (2010).
- [15] B. J. Eggleton, C. G. Poulton, P. T. Rakich, M. J. Steel, and G. Bahl, Brillouin integrated photonics, *Nat. Photonics* **13**, 664 (2019).
- [16] R. W. Boyd, *Nonlinear optics* (Academic Press, New York, 2020).
- [17] J. E. Sipe and M. J. Steel, A Hamiltonian treatment of stimulated Brillouin scattering in nanoscale integrated waveguides, *New J. Phys.* **18**, 045004 (2016).
- [18] V. Laude and J.-C. Beugnot, Lagrangian description of Brillouin scattering and electrostriction in nanoscale optical waveguides, *New J. Phys.* **17**, 125003 (2015).
- [19] P. Rakich and F. Marquardt, Quantum theory of continuum optomechanics, *New J. Phys.* **20**, 045005 (2018).
- [20] Z. Zhu, D. J. Gauthier, and R. W. Boyd, Stored light in an optical fiber via stimulated Brillouin scattering, *Science* **318**, 1748 (2007).
- [21] M. Merklein, B. Stiller, K. Vu, S. J. Madden, and B. J. Eggleton, A chip-integrated coherent photonic-phononic memory, *Nat. Commun.* **8**, 574 (2017).
- [22] B. Stiller, M. Merklein, C. Wolff, K. Vu, P. Ma, S. J. Madden, and B. J. Eggleton, Coherently refreshing hypersonic phonons for light storage, *Optica* **7**, 492 (2020).
- [23] B. Stiller, M. Merklein, K. Vu, P. Ma, S. J. Madden, C. G. Poulton, and B. J. Eggleton, Crosstalk-free multi-wavelength coherent light storage via Brillouin interaction, *APL Photonics* **4**, 040802 (2019).
- [24] A. H. Safavi-Naeini and O. Painter, Proposal for an optomechanical traveling wave phonon-photon translator, *New J. Phys.* **13**, 013017 (2011).
- [25] W. Chen and A. A. Clerk, Photon propagation in a one-dimensional optomechanical lattice, *Phys. Rev. A* **89**, 033854 (2014).
- [26] D. E. Chang, A. H. Safavi-Naeini, M. Hafezi, and O. Painter, Slowing and stopping light using an optomechanical crystal array, *New J. Phys.* **13**, 023003 (2011).
- [27] V. Peano, C. Brendel, M. Schmidt, and F. Marquardt, Topological Phases of Sound and Light, *Phys. Rev. X* **5**, 031011 (2015).
- [28] S. Walter and F. Marquardt, Classical dynamical gauge fields in optomechanics, *New J. Phys.* **18**, 113029 (2016).
- [29] Y.-C. Chen, S. Kim, and G. Bahl, Brillouin cooling in a linear waveguide, *New J. Phys.* **18**, 115004 (2016).
- [30] C. Wolff, M. J. A. Smith, B. Stiller, and C. G. Poulton, Brillouin scattering—Theory and experiment: Tutorial, *J. Opt. Soc. Am. B* **38**, 1243 (2021).
- [31] A. Nunnenkamp, K. Børkje, and S. M. Girvin, Single-Photon Optomechanics, *Phys. Rev. Lett.* **107**, 063602 (2011).
- [32] G. L. Keaton, M. J. Leonardo, M. W. Byer, and D. J. Richard, Stimulated Brillouin scattering of pulses in optical fibers, *Opt. Express* **22**, 13351 (2014).



- [33] Y.-D. Wang and A. A. Clerk, Using Interference for High Fidelity Quantum State Transfer in Optomechanics, *Phys. Rev. Lett.* **108**, 153603 (2012).
- [34] M. Dong and H. G. Winful, Area dependence of chirped-pulse stimulated Brillouin scattering: Implications for stored light and dynamic gratings, *J. Opt. Soc. Am. B* **32**, 2514 (2015).
- [35] Y. Xie, A. Choudhary, Y. Liu, D. Marpaung, K. Vu, P. Ma, D.-Y. Choi, S. Madden, and B. J. Eggleton, System-level performance of chip-based Brillouin microwave photonic bandpass filters, *J. Lightwave Technol.* **37**, 5246 (2019).
- [36] P. T. Rakich, C. Reinke, R. Camacho, P. Davids, and Z. Wang, Giant Enhancement of Stimulated Brillouin Scattering in the Subwavelength Limit, *Phys. Rev. X* **2**, 011008 (2012).
- [37] H. Shin, W. Qiu, R. Jarecki, J. A. Cox, R. H. Olsson, A. Starbuck, Z. Wang, and P. T. Rakich, Tailorable stimulated Brillouin scattering in nanoscale silicon waveguides, *Nat. Commun.* **4**, 1944 (2013).
- [38] K. S. Abedin, Single-frequency Brillouin lasing using single-mode As<sub>2</sub>Se<sub>3</sub> chalcogenide fiber, *Opt. Express* **14**, 4037 (2006).
- [39] P. Dainese, P. S. J. Russell, N. Joly, J. C. Knight, G. S. Wiederhecker, H. L. Fragnito, V. Laude, and A. Khelif, Stimulated Brillouin scattering from multi-ghz-guided acoustic phonons in nanostructured photonic crystal fibres, *Nat. Phys.* **2**, 388 (2006).
- [40] S. Le Floch and P. Cambon, Study of Brillouin gain spectrum in standard single-mode optical fiber at low temperatures (1.4–370 K) and high hydrostatic pressures (1–250 bars), *Opt. Commun.* **219**, 395 (2003).
- [41] R. O. Behunin, P. Kharel, W. H. Renninger, H. Shin, F. Carter, E. Kittlaus, and P. T. Rakich, Enhanced Brillouin scattering in silica via saturable phonon losses, in *Advanced Photonics 2015* (Optica Publishing Group, Washington, DC, 2015) p. IT4B.3.
- [42] I. Y. Dodin and N. J. Fisch, Storing, Retrieving, and Processing Optical Information by Raman Backscattering in Plasmas, *Phys. Rev. Lett.* **88**, 165001 (2002).
- [43] L. Tian and H. Wang, Optical wavelength conversion of quantum states with optomechanics, *Phys. Rev. A* **82**, 053806 (2010).
- [44] E. Verhagen, S. Deléglise, S. Weis, A. Schliesser, and T. J. Kippenberg, Quantum-coherent coupling of a mechanical oscillator to an optical cavity mode, *Nature (London)* **482**, 63 (2012).
- [45] Y.-C. Liu, Y.-F. Xiao, X. Luan, and C. W. Wong, Dynamic Dissipative Cooling of a Mechanical Resonator in Strong Coupling Optomechanics, *Phys. Rev. Lett.* **110**, 153606 (2013).
- [46] O. A. Nieves, M. D. Arnold, M. J. Steel, M. K. Schmidt, and C. G. Poulton, Numerical simulation of noise in pulsed Brillouin scattering, *J. Opt. Soc. Am. B* **38**, 2343 (2021).
- [47] C. M. de Sterke, K. R. Jackson, and B. D. Robert, Nonlinear coupled-mode equations on a finite interval: A numerical procedure, *J. Opt. Soc. Am. B* **8**, 403 (1991).
- [48] M. L. Citron, H. R. Gray, C. W. Gabel, and C. R. Stroud, Experimental study of power broadening in a two-level atom, *Phys. Rev. A* **16**, 1507 (1977).
- [49] L.-M. Duan, G. Giedke, J. I. Cirac, and P. Zoller, Inseparability Criterion for Continuous Variable Systems, *Phys. Rev. Lett.* **84**, 2722 (2000).
- [50] D. Vitali, S. Gigan, A. Ferreira, H. R. Böhm, P. Tombesi, A. Guerreiro, V. Vedral, A. Zeilinger, and M. Aspelmeyer, Optomechanical Entanglement Between a Movable Mirror and a Cavity Field, *Phys. Rev. Lett.* **98**, 030405 (2007).
- [51] S. G. Hofer, W. Wiczorek, M. Aspelmeyer, and K. Hammerer, Quantum entanglement and teleportation in pulsed cavity optomechanics, *Phys. Rev. A* **84**, 052327 (2011).
- [52] L. Tian, Robust Photon Entanglement Via Quantum Interference in Optomechanical Interfaces, *Phys. Rev. Lett.* **110**, 233602 (2013).
- [53] M. C. Kuzyk, S. J. van Enk, and H. Wang, Generating robust optical entanglement in weak-coupling optomechanical systems, *Phys. Rev. A* **88**, 062341 (2013).
- [54] D. Hatanaka, I. Mahboob, K. Onomitsu, and H. Yamaguchi, Phonon waveguides for electromechanical circuits, *Nat. Nanotechnol.* **9**, 520 (2014).
- [55] See Supplemental Material at <http://link.aps.org/supplemental/10.1103/PhysRevResearch.5.013010> for the data and source codes for all the figures.